

**Aus der Universitäts-Augenklinik Tübingen
Abteilung Augenheilkunde II
Ärztlicher Direktor: Professor Dr. E. Zrenner**

**Studying the L- and M-cone ratios by the multifocal
visual evoked potential**

**Inaugural-Dissertation
zur Erlangung des Doktorgrades
der Medizin**

**der Medizinische Fakultät
der Eberhard-Karls-Universität
zu Tübingen**

**vorgelegt von
Alice Lap-Ho Yu
aus
Hongkong**

2005

Dekan:

Professor Dr. C. D. Claussen

1. Berichterstatter:

Professor Dr. E. Zrenner

2. Berichterstatter:

Professor Dr. H. – P. Thier

To my parents

TABLE OF CONTENTS

| | | |
|------------|--|-----------|
| 1 | Introduction | 1 |
| 1.1 | Physiology of Color Vision | 3 |
| 1.1.1 | Morphology of Cones | 3 |
| 1.1.2 | Spatial Distribution of Cones | 4 |
| 1.1.3 | Processing of Visual Signals in the Retina | 4 |
| 1.1.4 | Ganglion Cells and the MC and PC Pathways | 6 |
| 1.1.5 | Red-green and Luminance Pathways | 8 |
| 1.2 | Significance of the Relative Number of L- and M-cones | 10 |
| 1.3 | Multifocal Visual Evoked Potential (mfVEP) | 12 |
| 1.4 | Multifocal Stimulation | 13 |
| 1.5 | Silent Substitution Technique | 14 |
| 1.6 | Thesis Goals | 15 |
| 2 | Materials and Methods | 16 |
| 2.1 | Subjects | 16 |
| 2.2 | L- and M-cone Isolation for the mfVEP | 17 |
| 2.2.1 | Calibration of the mfVEP Monitor | 17 |
| 2.2.2 | Cone Fundamentals | 18 |
| 2.2.3 | Silent Substitution | 19 |
| 2.2.4 | L-cone Modulation for the mfVEP | 22 |

| | | |
|------------|---|-----------|
| 2.2.4.1 | L-cone Quantal Catch in the L-cone Modulation | 24 |
| 2.2.4.2 | M-cone Quantal Catch in the L-cone Modulation | 25 |
| 2.2.4.3 | Cone Contrast for the L-cone Modulation | 26 |
| 2.2.5 | M-cone Modulation for the mfVEP | 27 |
| 2.2.5.1 | M-cone Quantal Catch in the M-cone Modulation | 28 |
| 2.2.5.2 | L-cone Quantal Catch in the M-cone Modulation | 29 |
| 2.2.5.3 | Cone Contrast for the M-cone Modulation | 29 |
| 2.3 | L- and M-cone Isolation for the mfERG | 30 |
| 2.4 | Multifocal Visual Evoked Potential (mfVEP) | 31 |
| 2.4.1 | Hardware and Software | 31 |
| 2.4.2 | Multifocal Stimulation in the mfVEP | 33 |
| 2.4.3 | mfVEP Stimulus Calibration | 35 |
| 2.4.4 | Electrode Placement and Three Channels | 35 |
| 2.4.5 | mfVEP Recording Parameters | 36 |
| 2.4.6 | mfVEP Recording Protocol | 36 |
| 2.5 | Multifocal Electroretinogram (mfERG) | 37 |
| 2.5.1 | Hardware and Software | 37 |
| 2.5.2 | Multifocal Stimulation in the mfERG | 38 |
| 2.5.3 | mfERG Stimulus Calibration | 39 |
| 2.5.4 | mfERG Electrodes | 39 |
| 2.5.5 | mfERG Recording Parameters | 40 |
| 2.5.6 | mfERG Recording Protocol | 40 |
| 3 | Results | 42 |
| 3.1 | Test Studies for the L- and M-cone Modulation Settings | 42 |
| 3.1.1 | Dichromat Data | 42 |
| 3.1.2 | Cone Fundamentals for 2° | 42 |

| | | |
|------------|--|-----------|
| 3.2 | mfVEP Studies | 43 |
| 3.2.1 | General Features of VEP Responses | 43 |
| 3.2.2 | Displaying the mfVEP Responses | 44 |
| 3.2.3 | Grouping of the mfVEP Responses | 47 |
| 3.2.4 | Comparison of the Central to Middle/Peripheral Groups | 48 |
| 3.2.5 | Root Mean Square (RMS) Ratio | 51 |
| 3.2.6 | Comparison of mfVEP Responses Summed in Six Rings | 53 |
| 3.2.7 | Effects of Contrast | 54 |
| | | |
| 3.3 | mfERG Studies | 58 |
| 3.3.1 | General Features of ERG Responses | 58 |
| 3.3.2 | Summed mfERG Responses to L- and M-cone Modulation | 58 |
| | | |
| 4 | Discussion | 60 |
| | | |
| 4.1 | Method Discussion | 60 |
| 4.1.1 | Reliability of the L- and M-cone Isolating Stimuli | 60 |
| 4.1.2 | Difficulties in the mfVEP Recordings | 61 |
| 4.1.3 | Difficulties in the mfERG Recordings | 62 |
| | | |
| 4.2 | Discussion of the Results | 63 |
| 4.2.1 | Foveal mfVEP and PC Pathway | 63 |
| 4.2.2 | Peripheral mfVEP and MC Pathway | 66 |
| 4.2.3 | Limitations of the mfVEP for L/M-cone Ratio Estimates | 67 |
| 4.2.4 | Effects of Contrast Changes in the mfVEP | 67 |
| 4.2.5 | Interpretation of the mfERG Results | 69 |
| | | |
| 4.3 | Discussion of Various Techniques for L/M-cone Ratio Estimates | 70 |
| 4.3.1 | Heterochromatic Flicker Photometry (HFP) | 70 |
| 4.3.2 | Retinal Densitometry | 72 |

| | | |
|------------|---|-----------|
| 4.3.3 | Flicker-photometric ERG | 73 |
| 4.3.4 | mRNA Analysis | 74 |
| 4.3.5 | Direct High-resolution Imaging of the Retina | 74 |
| 4.3.6 | Microspectrophotometry of Single Cones | 75 |
| 4.3.7 | Monochromatic Light Detection | 75 |
| 4.3.8 | Detection of Unique Yellow | 76 |
| 4.3.9 | Foveal Cone Detection Thresholds | 77 |
| 4.3.10 | Red-green Equiluminance Points | 77 |
| 4.3.11 | Flicker Detection Thresholds and Minimal Flicker Perception | 78 |
| 4.4 | Conclusion | 79 |
| 5 | Summary | 80 |
| 6 | Appendix | 82 |
| 6.1 | Screen Calibration Table | 82 |
| 6.2 | Index of Figures | 83 |
| 6.3 | Index of Tables | 84 |
| 7 | References | 85 |

1 Introduction

„ Now, as it is almost impossible to conceive each sensitive point of the retina to contain an infinite number of particles, each capable of vibrating in perfect unison with every possible undulation, it becomes necessary to suppose the number limited, for instance, to the three principal colours, red, yellow, and blue, of which the undulations are related in magnitude nearly as the numbers 8, 7, and 6; and that each of the particles is capable of being put in motion less or more forcibly by undulations differing less or more from a perfect unison; for instance the undulations of green light being nearly in the ratio of 6 1/2, will affect equally the particles in unison with yellow and blue, and produce the same effect as a light composed of these two species: and each sensitive filament of the nerve may consist of three portions, one for each principal colour.“ (Young 1802)

With this observation in 1802, the British physicist Thomas Young suggested that the retina might be sensitive to only three principal colors, and that the sensation of different colors might depend on varying degree of excitation of these three receptors. This model of color perception laid the groundwork for the trichromatic theory of color vision: Human color vision is initiated by absorption of light by three different classes of cone receptors, and all colors of the visible spectrum can be matched by appropriate mixing of three primary colors. Consequently, trichromacy is not attributable to the spectral composition of the light but to the biological limitation of the eye. Later on, in 1852, Hermann von Helmholtz, a German physiologist, stated that our ability of color detection is based on a comparison of the relative outputs of the three cone types at some postreceptoral stage:

„Luminous rays of different wavelength and colour distinguish themselves in their physiological action from tones of different times of vibration, by the circumstance that every two of the former, acting

simultaneously upon the same nervous fibres, give rise to a simple sensation in which the most practised organ cannot detect the single composing elements, while two tones, though exciting by their united action the peculiar sensation of harmony or discord, are nevertheless always capable of being distinguished singly by the ear. The union of the impressions of two different colours to a single one is evidently a physiological phenomenon, which depends solely upon the peculiar reaction of the visual nerves. In the pure domain of physics such a union never takes place objectively. Rays of different colours proceed side by side without any mutual action, and though to the eye they may appear united, they can always be separated from each other by physical means.“
(von Helmholtz 1852)

Since then, the modern version of the Young-Helmholtz theory of trichromacy has been based on the premise that there are three classes of cone receptors, each containing a different photopigment in their outer segments. They are named L, M, and S (long-, middle- and short-wavelength sensitive, respectively) according to the part of the visible spectrum to which they are most sensitive. The spectral sensitivity of each cone type can exactly be measured by the device of a microspectrophotometry, which reveals that S-cones peak at approximately 437 nm, M-cones peak at 533 nm and L-cones peak at 564 nm (Gouras 1984).

Vision is initiated by a transduction process starting in the retina with its photopigment absorbing a photon. The probability of a photon being absorbed depends on both the wavelength and the density of the photons incident on the photoreceptor. Therefore the coding for wavelength, and thus color detection, arises from comparison of the relative excitatory signals of each cone type at some postreceptoral sites. The processing of cone signals itself, beginning in the retina and continuing to the cerebral cortex of the brain, is a very complex chapter of color vision. In order to understand the physiology of color vision and to study the interconnections and responses of neurons, it is fundamental to

know about the morphology, the spatial distribution and the relative numbers of cones.

1.1 Physiology of Color Vision

1.1.1 Morphology of Cones

In the mammalian retina, photoreceptors can be divided into rods and cones; rods to detect dim light and cones to mediate color vision. Their names are derived from their lightmicroscopical structure: Cones are robust conical-shaped structures with their cell bodies situated in a single row directly below the outer limiting membrane, and rods are slim rod-shaped structures filling the area between the larger cones. A photoreceptor consists of four major functional regions:

- an outer segment filled with stacks of folded double membrane, which contain the visual pigment molecules (rhodopsins), and where phototransduction occurs.
- an inner segment containing mitochondria, ribosomes and membranes, where biosynthesis of opsins occurs (a thin cilium joins the inner and outer segments of the photoreceptors).
- a cell body containing the nucleus of the photoreceptor cell.
- a synaptic terminal, where neurotransmission to second order neurons occurs.

The visual pigment molecules, which initiate the phototransduction process, are embedded in the bilipid membranous discs forming the outer segment. The visual pigment molecules, namely rhodopsins, consist of the protein opsin and the light-absorbing chromophore 11-cis retinal. Each molecule of rhodopsin is made up of seven transmembrane portions surrounding the 11-cis retinal, which apparently lies horizontally in the membrane and is bound at a lysine residue to the helix seven.

1.1.2 Spatial Distribution of Cones

Photoreceptors are organized in a mosaic pattern. In the fovea, L- and M-cones are randomly distributed in a fairly regular hexagonal mosaic, which is only distorted by large-diameter S-cones. Thus, cluster of the same type of cones may occur. Rods are missing in the foveal pit. Their density is highest in a ring around the fovea at about 4.5 mm or 18 degrees from the foveal pit (Osterberg 1935). Outside the fovea, the hexagonal packing of the cones is broken up by the rods. The optic nerve (blind spot) is free of photoreceptors.

The cone density is highest in the foveal pit and falls rapidly outside the fovea to a fairly even density into the peripheral retina (Curcio et al. 1987). The S-cones form about 8-12% of the cones in the fovea, with their lowest density at 3-5% of the cones in the foveal pit and their highest density at 15% on the foveal slope (1 degree from the fovea pit). Outside the fovea, they make up about 8% of the total cone population, evenly scattered between the hexagonal packing of the other two cones (Ahnelt et al. 1987). The L- and M-cones form about 88-92% of the cones in the fovea, and about 92% of the cones outside the fovea. Their relative numbers are discussed later in this study.

1.1.3 Processing of Visual Signals in the Retina

The processing of visual signals begins in the photoreceptors, which absorb the photons of the light and convert them into electrical energy. On the biochemical level, the following enzyme cascade occurs: Light activates rhodopsin, which induces an isomerization of retinal from the 11-cis form to an all-trans form, which in turn causes a semistable conformation change of opsin and a release of several intermediaries - among them metarhodopsin II. Metarhodopsin II stimulates transducin, a G protein, which in turn activates cGMP phosphodiesterase. Consequently, the cytoplasmic concentration of cGMP drops, and the cGMP-gated ion channels in the outer segment membrane of the photoreceptors close. In the dark, a steady current flows into open cGMP-gated ion channels, allowing an inward current of Na^+ , and thus depolarizing the photoreceptor cells. When light stimulates the rhodopsin molecules and above cascade ensues, the closure of the cGMP-gated ion

channels results in a drop of the Na^+ inward current, and thus in a hyperpolarization of the photoreceptor cells and a decrease in the release of the neurotransmitter glutamate.

The receptive field of a visual neuron is defined as the retinal area, whose stimulation activates this visual neuron. It is set in a concentric arrangement, consisting of a receptive field center and a receptive field surround. The size of receptive fields increases from the fovea to the periphery, and the receptive fields of neighbouring neurons overlap each other. The function and size of receptive fields can be explained by the synaptic signal convergence and divergence in the neuronal cells of the retina. In the retina, a signal can traverse directly from the photoreceptors to the bipolar cells and ganglion cells and thus activates the receptive field center, or it can be transmitted from the photoreceptors via interneurons, namely horizontal cells and amacrine cells, to the bipolar cells and ganglion cells and thus activates the receptive field surround. The activation of the receptive field center can cause depolarization or hyperpolarization, depending on the synaptic neurotransmitter released between the cones and the bipolar cells. However, the response to the surround is always of opposite sign than to the center of the receptive field, achieved via lateral inhibitions of bipolar cells by horizontal cells (Kaneko 1970). In this way, this center-surround organization of the receptive field creates simultaneous contrast, needed for high resolution.

One pattern of the ganglion cell receptive field is the ON-center, OFF-surround pattern. Light hitting the center of the receptive field depolarizes the ganglion cell, while light hitting the surround of the receptive field hyperpolarizes the ganglion cell. OFF-center, ON-surround is the other possible pattern, where the responses of the ganglion cells are reversed. These two patterns can already be found at earlier stages of cone signal transmission. Thus, the processing of cone signals occurs in two parallel channels, which have the function of mediating successive contrast. They are called ON-center channel - providing information of brighter than background stimulus - and OFF-center channel - providing information of darker than background stimulus (Kuffler 1953). Each channel comprises bipolar and ganglion cells, with the ON-center

channel excited by an increment of light absorption, and the OFF-center channel excited by the decrement of light absorption.

The origins of the ON- and OFF-center channels are determined by the synaptic contacts of bipolar cells with the cone pedicles, since the synapses between the bipolar and ganglion cells only conduct excitatory signals: On the one hand, there are the invaginating bipolar cells, which connect with the cone pedicles via central invaginating dendrites at ribbon synapses in the cone pedicles. They are related to metabotropic glutamate receptors (mGluR), selectively sensitive to the glutamate agonist APB (or AP4, 2-amino-4-phosphonobutyrate), which hyperpolarizes the membrane potentials. Thus, the invaginating bipolar cells depolarize with lightness and form the start of ON-center channels. On the other hand, there are the flat bipolar cells, which contact the cone pedicles by means of semi-invaginating, wide-cleft basal junctions and carry AMPA-kainate receptors, which are excitatory, ionotropic glutamate receptors (iGluR). Therefore the flat bipolar cells hyperpolarize with lightness and thus make up the start of OFF-center channels (Nelson and Kolb 1983). These bipolar responses are transmitted to ganglion cells with dendrites of anatomically separated sublaminae of the inner plexiform layer (Famiglietti and Kolb 1976). The invaginating bipolar cells of the ON-center channels contact ganglion cells with dendrites in the sublamina b (proximal retina), whereas the flat bipolar cells of the OFF-center channels are connected to dendrites of ganglion cells within the sublamina a (distal retina). This specificity of bipolar to ganglion cell contacts, underlying ON-center and OFF-center ganglion cell responses, was first described in monkeys (Gouras 1971). Later, this hypothesis was conclusively proved by means of intracellular recordings in ganglion cells of cat (Nelson et al. 1978).

1.1.4 Ganglion Cells and the MC and PC Pathways

In the human retina, the ganglion cells can be divided into 18 or more different morphological types. However, there are only three different ganglion cell types, which are involved in the human color processing system: the midget ganglion cells, the parasol ganglion cells and the small bistratified ganglion

cells. Most of these ganglion cell types project to the Lateral Geniculate Nucleus (LGN) by the following two distinctive pathways: the MC and PC pathways.

The concept of the MC and PC pathways is termed according to the laminae within the primate LGN, in which ganglion cell axons terminate. The LGN is divided into six separate layers of cells: The four dorsal layers comprise of small neurons, therefore they are named the parvocellular layers. The two ventral layers are made up by larger cells and therefore are called the magnocellular layers. These different types of LGN layers receive input from different types of ganglion cells. These ganglion cells were first characterized by Polyak (1941), who named them as parasol ganglion cells and midget ganglion cells. Parasol ganglion cells are identified as the M cells, projecting to the magnocellular LGN (Perry et al. 1984). They are fewer in number, but each cell has a large, branched dendritic field and a large axon. In contrary, the midget ganglion cells are the anatomical counterpart of the P cells, feeding into the parvocellular LGN layers (Merigan 1989). They show small compact dendritic fields and smaller axons.

Neurons in both MC and PC pathways are also mostly different in their physiological characteristics. Parasol ganglion cells of the retina and the LGN are highly sensitive to luminance contrast and have a high contrast gain. They are especially sensitive to low contrast stimuli but saturate already at low contrast level (10-15%) (Derrington and Lennie 1984; Purpura et al. 1988; Scar et al. 1990). In addition, the parasol ganglion cells apparently play an important role in transmitting information about the high temporal and low spatial frequencies in the stimuli (Derrington and Lennie 1984). Therefore they are useful for the perception of high frequency flicker (Schiller and Colby 1983; Lee et al. 1990; Benardete et al. 1992) and motion (Schiller et al. 1991). In contrary, the midget ganglion cells of the retina and the LGN are mainly responsible for color detection. They are spectrally opponent and form the red-green axis, by receiving antagonistic inputs from both L- and M-cones, and the blue-yellow axis, by opposing the S-cones to a combined signal from L- and M-cones (Krauskopf et al. 1982). The midget ganglion cells are therefore highly sensitive

to chromatic contrast and saturate at a much higher contrast level. However, their contrast gain is relatively low (Derrington and Lennie 1984; Purpura et al. 1988; Scar et al. 1990). They prefer to detect high spatial but low temporal frequencies in the stimuli (Derrington and Lennie 1984), which is mostly important for color, texture and pattern discrimination and high visual acuity (Derrington et al. 1984; Merigan 1989; Schiller et al. 1991; Lynch et al. 1992).

A distinctive pathway in color vision includes the small bistratified ganglion cells, which project to intercalated cells between the magnocellular and parvocellular layers of the LGN (Martin et al. 1997; White et al. 1998). Their inner dendritic trees synapse with the blue cone bipolar cells, which themselves are exclusively connected to S-cones (Kouyama and Marshak 1992). Their outer dendritic trees are stratified in the amacrine cell layer, which in turn receives input from non-selective L- and M-cones (Dacey and Lee 1994; Calkins et al. 1998). The small bistratified ganglion cells are reserved to carry color information. They belong to the short-wavelength system, which is more sensitive to lower spatial and temporal frequencies than the other two cone systems.

Besides the MC and PC pathways, there is a third retinogeniculocortical pathway, the so-called koniocellular (KC) pathway. The KC pathway conveys information of moving stimuli via the LGN to the cortex. The K cells, feeding into the KC pathway, are a physiologically heterogeneous group in terms of their temporal and spatial sensitivities. Though overall, it is assumed that the response properties of K cells are more similar to those of P cells than those of M cells (Solomon et al. 1999).

1.1.5 Red-green and Luminance Pathways

Parasol and midget ganglion cells together make up about 90% of the total retinal ganglion cells, with 10% being parasol and 80% being midget ganglion cells. Parasol and midget ganglion cells have a characteristic distribution within the retina: Dacey and Peterson (1992) examined the dendritic field sizes of parasol and midget ganglion cells by using intracellular staining in an in vitro preparation of a isolated and intact human retina. In the human fovea, the

midget ganglion cells make up about 90%, parasol ganglion cells about 5% and small bistratified ganglion cells about 1%. Opposed to that, the proportion of the midget ganglion cells in the peripheral retina lies around 45%, parasol ganglion cells about 20% and small bistratified ganglion cells about 10%. Thus, unlike the parasol and small bistratified ganglion cells, the midget ganglion cells are most densely populated in the parafoveal retina and decrease in number with eccentricity.

In the parafoveal retina, extending over the central 7-10° eccentricity, the midget ganglion cells make up special cone pathways, the so-called midget pathways. In a midget pathway, only one cone connects to one bipolar cell to one ganglion cell through a private-line, to provide maximal resolution capabilities and visual acuity (Kolb and Dekorver 1991; Calkins et al. 1994). In order to ensure high contrast discrimination, also the midget pathway is organized in two parallel channels: Every cone is connected to two midget bipolar cells, one bipolar cell of an ON-center type connected to an ON-center ganglion cell, and one bipolar cell of an OFF-center type connected to an OFF-center ganglion cell (Kolb 1970). These midget pathways form the substrate for the circuitry for red-green opponency. As the private-line persists through the midget-single-cone pathway, the midget system of L- and M-cones carries sensitivity information of its wavelength in its receptive field center to the brain, where further processing occurs for final color discrimination.

However, with increasing eccentricities to the periphery, the midget ganglion cells increase in their dendritic tree dimension (Dacey 1993) and therefore are connected to an increasing number of multibranching midget bipolar cells (Milam et al. 1993), which themselves receive input from multiple cones. It is still questionable if these multibranching midget bipolar cells stay committed to one spectral class of cone or transmit a mixture of chromatic types. According to the cone-type mixed hypothesis, L- and M-cones are randomly connected to the midget receptive field (Lennie et al. 1991; De Valois and De Valois 1993; Mullen and Kingdom 1996). Therefore cone-type selectivity can only occur, when cone input to the receptive field center is restricted to one cone and dominates over a mixed-cone input to a weaker surround. For this reason, the

midget pathways in the parafovea account for a strong red-green opponency. In contrary to that, with increasing dendritic field size of midget ganglion cells in the retinal periphery, both the receptive field center and surround receive input from both L- and M-cones, resulting in a non-opponent light response (Dacey 1999).

The parasol ganglion cells, on the other hand, increase in number from the fovea to the periphery and show no private-line pathways. They have large cell bodies with a large extension of dendrites, which are connected to diffuse bipolar cells (Jacoby et al. 1996). Those diffuse bipolar cells converge signals from multiple cones (Dacey et al. 2000b). Although they are anatomically linked with the S-cones, S-cone contribution is neglectable. Thus, the parasol ganglion cells draw indiscriminate inputs from L- and M-cones to both their receptive field center and surround, similar to the midget ganglion cells in the periphery. Thus, they carry non-opponent signals, known to create the luminance pathways, which are driven by both L- and M-cone signals.

1.2 Significance of the Relative Number of L- and M-cones

In the evolution of color vision, two different cone types have evolved, one best responding to one part and the other to the other part of the visible spectrum, namely the L-cones and S-cones, so that the brain could compare both signals to distinguish color. With the emergence of trivariant human color vision, the long-wavelength system has been split into two similar systems with similar opsins, which are sensitive to slightly different spectral sensitivities, one most sensitive to yellow-green and the other to yellow-red. Molecular analysis has shown that L- and M-cone photopigment gene loci are located in a tandem array on the X chromosome, and that the amino acid sequences for these two proteins are nearly identical (Nathans et al. 1986a,b). By this duplication, both L- and M-cones use the same neural circuitry, compared to the S-cones with their own neural pathways. Furthermore, S-cones are morphologically distinct (Ahnelt et al. 1990; Calkins et al. 1998) and spatially form an independent and

non-random arrangement across the retina (Curcio et al. 1991). By contrast, the L- and M-cones cannot be distinguished morphologically (Wikler and Rakic 1990). As L- and M-cones also do not appear to be recognized selectively by each other (Tsukamoto et al. 1992) or by the bipolar cells, it is essential to know the spatial arrangement and relative number of L- and M-cones across the retina in order to understand the pathways for luminance and red-green opponency. Studying the proportions of cones also provides a better understanding about how postreceptoral pathways may adjust to the large variability of cone ratios, and how the variability of cone ratios affects color perception among individuals. This and more can provide deeper insights into the visual capacity of the human eye.

It seems to be acknowledged, that the number of L- to M-cones in the human retina varies widely among individuals. For the foveal L/M-cone ratios, estimates were obtained by fitting HFP functions with weighted sum of L- and M-cone fundamentals and yielded an average ratio of 1.5 to 2.0 (Guth et al. 1968; Vos and Walraven 1971; Smith and Pokorny 1975; Stockman and Sharpe 2000). Other psychophysical techniques, like the point-source detection technique, gave estimates ranging from 1.6:1 to greater than 7:1 (Wesner et al. 1991; Otake and Cicerone 2000). Flicker-photometric ERGs suggested a ratio between 0.6:1 and 12:1 (Jacobs et al. 1996; Carroll et al. 2000). Recordings by the multifocal electroretinogram (mfERG) with cone-isolating stimuli brought up similar data (Kremers et al. 1999; Albrecht et al. 2002), as did the combination of psychophysical tasks, ERGs and retinal densitometry (Kremers et al. 2000). Already the sole application of retinal densitometry suggested a large variation of cone numbers (Rushton and Baker 1964). New approaches with direct retinal imaging provided convincing results of very diverse L/M-cone ratio of 1.15:1 and 3.79:1 for two color normal subjects (Roorda and Williams 1999). Analysis of the L/M-cone pigment mRNA revealed ratios between 4.3:1 and 6.7:1 (Hagstrom et al. 2000).

Thus, there seems to be general agreement, that there are more L- than M-cones in the human retina and there is evidence indicating that the L/M-cone ratios of individuals may vary from less than 1:1 to more than 10:1. However, it

is still unclear, if there are any changes in the L/M-cone ratio with eccentricity. Examinations of the L/M-cone pigment mRNA in retinal patches of 23 human donor eyes elicited an average L/M cone ratio of 1.5:1 for the central retina, and a ratio up to 3:1 for the retinal periphery of approximately 40° eccentricity (Hagstrom et al. 1998). An accompanying mfERG study (Albrecht et al. 2002) suggested similar results with a lower L/M cone ratio in the central fovea (5° diameter) than in the periphery (annular ring centered at 40°). However, here the resolution of the central foveal region was limited to about 5° in diameter. In contrast to that, analysis of the L/M cone photopigment mRNA ratio in the whole retinas of Old World monkeys showed no change in this ratio with eccentricity up to 9 mm (~45°) (Deeb et al. 2000). The L/M mRNA ratios among these nonhuman primates, however, were also highly variable between 0.6 to 7.0.

1.3 Multifocal Visual Evoked Potential (mfVEP)

The visual evoked potential (VEP) is a gross electrical potential generated from activated cells in the primary visual cortex in the occipital lobe. A stimulus, which is presented to the subject's vision, produces electrical potentials in the neuro-optical pathway traveling from the retina to the primary visual cortex. Electrodes are placed at the scalp directly above the occipital cortex in order to record the VEPs, which are used to examine the visual pathway from the retina via the optic nerve, the chiasma, the optic radiation to the area 17. The techniques most commonly used are the flash and pattern reversal VEP. Optimal recordings with pattern reversal VEP can only be obtained with correct refraction. Therefore, pattern reversal VEPs find use in determining objective refraction (Teping et al. 1981), especially in cases of unknown visual loss with intact retinal functions. Besides that, the VEP is sensitive to demyelinating or inflammatory optic nerve diseases, and therefore it is used in the diagnosis of multiple sclerosis or precisely optic neuritis. It has been shown that approximately two-third of multiple sclerosis patients present with delayed VEP implicit times with or without impaired vision (Halliday et al. 1973).

1.4 Multifocal Stimulation

The VEP signal comprises inputs from multiple visual areas of the brain and therefore is a summed response of all these visual representations. To extract the different components of the neural mechanisms responsible for the total VEP signal, it is necessary to stimulate specific cortical sources separately. This has been a complex task, since reducing the size of the stimuli was limited by a poor signal-to-noise ratio of the VEP responses, and repeated recordings from many locations required many recording sessions, making a comparison of signals impossible. Baseler et al. (1994) presented a solution by applying the multiple-input method to the recording of VEPs, which was firstly developed by Sutter and Tran (1992) for the study of the field topography of ERG responses. This multifocal technique allows a simultaneous recording of 60 or more independently stimulated local VEP responses across the visual field. To overcome the great variations in gross cortical anatomy among individuals, stimuli are scaled with eccentricity according to the cortical magnification in human striate cortex (V1).

The initial conclusion of Baseler et al. (1994), that clinical field testing with the mfVEP would not be feasible due to its great inter-subject variability, was soon dismissed by the hypothesis of Klistorner et al. (1998), suggesting a close correspondence between the mfVEP and the Humphrey visual field defects. A new approach to overcome the inter-subject variability in the mfVEP responses was laid down by Hood et al. (2000b), who compared monocular mfVEP responses from both eyes of the same patient. Since then, clinical use of the mfVEP has been established. So can local damage to the optic nerve be detected by decreased VEP amplitudes. In ischemic optic neuropathy, the reduction in amplitude correlates with the degree of visual field loss, whereas the implicit time remains unchanged (Hood and Zhang 2000). Changes in the VEP of optic neuritis patients present differently at the onset and after recovery: While at the onset amplitude decreases and implicit time is prolonged, the recovery from optic neuritis is marked by a regain of full amplitude in all regions,

while the implicit time in the affected regions of visual field loss during the acute phase remains prolonged (Hood et al. 2000a).

1.5 Silent Substitution Technique

Estevez and Spekreijse (1982) firstly described a method of silent substitution, formerly called spectral compensation, in 1974, in which one of the cones is selectively stimulated, while the other cones are kept from responding to the stimulus. This method was based on the 'principle of univariance' of Rushton, saying that for each class of cones the result of light depends upon the effective quantal catch, but not upon what quanta are caught (Mitchell and Rushton 1971a,b). Rushton introduced the concept of effective quantal catch, which is the fraction of the quantal flux from a light source that actually produces pigment bleaching. Thus, only the amount of bleaching (and not e.g. the amount of quanta caught in a cone by passive pigments or transition photoproducts) leads to an intrinsic response of a cone contributing to a real visual response.

In the principle of trichromacy, any spectral light can be matched by a mixture of three fixed-color primary lights ('primaries'). The match is achieved when the amount of total quantal catch, which the three primaries produce in each of the three cone types, equals to the quantal catch produced by the spectral test light. Similarly, there are spectral test lights, which are equally effective for two spectrally different lights, meaning that the two lights are color-matched and metameric in their two mechanisms and cannot be distinguished from each other by our visual system. Thus, a substitution can be detected for the third non-metameric light. This is the basic idea behind the silent substitution method, which uses the linearity of color-matching processes (Grassmann's laws) and the trichromacy of color vision to calculate the effective quantal catch in the cone pigments. The cone-isolating stimulus is a spectral light, which only modulates a single cone type and is determined by the total effective quantal catch in the pigments of this cone type.

1.6 Thesis Goals

The goals of our study were to examine the underlying mechanisms for cone signal processing with regard to the L/M-cone ratio in the central fovea and to compare them with peripheral visual processing. The mfVEP technique appeared to be a particularly good way to study the central fovea, since the mfVEP is generated after foveal responses has been cortically magnified.

In the first part of our study, we calculated the stimulus settings for the L-cone and M-cone-isolating stimuli in accordance with the silent substitution method. To ensure the reliability of our calculated cone-isolating stimuli, we adjusted the stimulus settings to the mfVEP recordings from a protanopic and deuteranopic observer.

In the second part of our study, we conducted mfVEP recordings for 50% L-cone modulation and 50% M-cone modulation on six color-normal trichromats. These mfVEP recordings should provide deeper insights into the L/M-cone ratio in the central 1.2° of visual field and bring up the difference between central and peripheral visual processing.

In the third part of our study, we examined the effect of contrast reductions in the mfVEP responses to L- and M-cone modulations, with the aim to see if any change in the relative strengths of L- and M-cone input was revealed in the mfVEP responses.

In the fourth part of our study, we compared the mfVEP responses of two observers with their mfERG data previously obtained in Tübingen, Germany in order to have a closer look at the cone pathways in the central fovea, where normalization mechanisms for the L/M-cone ratio were suspected.

2 Materials and Methods

2.1 Subjects

In this study, we had six subjects with a 20/20 corrected visual acuity and normal color vision with no history of color blindness in their pedigree. Normal color vision was obtained by the Ishihara pseudoisochromatic plates and Nagel Type I anomaloscope. In one male (DH) and two females (AY and CC), we did molecular genetic (DNA) analysis of their venous blood. All of the three samples showed a normal L-cone pigment gene (1st gene in the array) and one or more normal M-cone pigment genes (downstream) on the X-chromosomes, but no L/M or M/L hybrid genes. Thus, both females were very unlikely to be carriers of any protan or deutan color-vision deficiencies, since they only had normal L- and M-cone pigment genes on their two X-chromosomes.

Informed consent was obtained from all subjects before their participation. This study was conducted in accordance with the tenets of the Declaration of Helsinki. It was approved by the committee of the Institutional Board of Research Associates of Columbia University, New York, NY, U.S.A. and by the Institutional Ethics Committee in Human Experimentation at the University of Tübingen, Germany.

Table 1. Subject information

| Subject | Age | Gender | Eye | Visual Acuity |
|---------|-----|--------|-----|---------------|
| AY | 24 | f | OS | 20/20 |
| CC | 25 | f | OD | 20/20 |
| DH | 58 | m | OS | 20/20 |
| KS | 16 | f | OS | 20/20 |
| NK | 21 | f | OD | 20/20 |
| XZ | 31 | m | OD | 20/20 |

2.2 L- and M-cone Isolation for the mfVEP

2.2.1 Calibration of the mfVEP Monitor

The calibration of the display monitor was performed under the same conditions like the experiments of this study themselves. The maximum intensities of red, green and blue phosphors, which the monitor could produce on the screen, were displayed, and the emission spectra of each phosphor were then measured by a compact array spectroradiometer (CAS 140, Instrument Systems GmbH, München, Germany). These emission spectra are depicted in the graphs below: The red phosphor had its primary peak at 626 nm and a secondary peak at 706 nm. The green phosphor had its peak at 514 nm, and the blue phosphor at 448 nm. The maximum intensities of the red, green and blue phosphors were 22.7, 72.2, and 10.3 cd/m^2 , respectively.

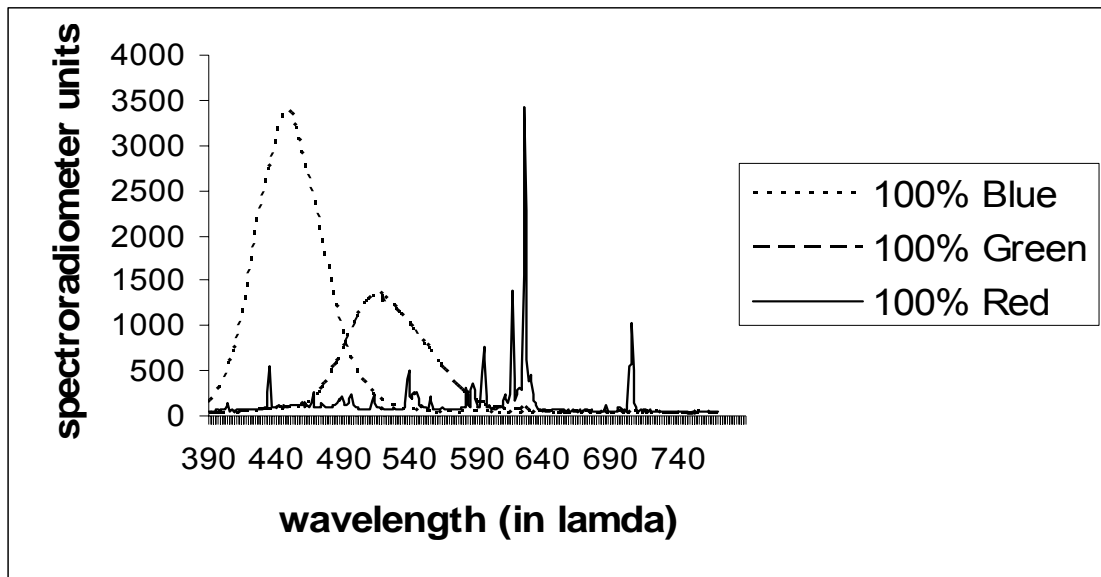


Figure 1. Emission spectra of the three phosphors as measured by the spectroradiometer.

The spectroradiometer displayed in units of $\text{J} \cdot \text{s}^{-1} \cdot \text{m}^{-2} \cdot \text{nm}^{-1}$ (Joule per second per square meter per nanometer). With the Planck's formula for radiant energy, the number of quanta n could be calculated:

$$E = n \cdot h \cdot \nu$$

$$E = n * h * c / \lambda$$

$$n = (E * \lambda) / (h * c)$$

where E is the phosphor's energy, n the number of quanta, h the Planck's constant ($6.626 * 10^{-34}$ J*s), ν the frequency, c the speed of light ($300,000$ km * s⁻¹) and λ the wavelength.

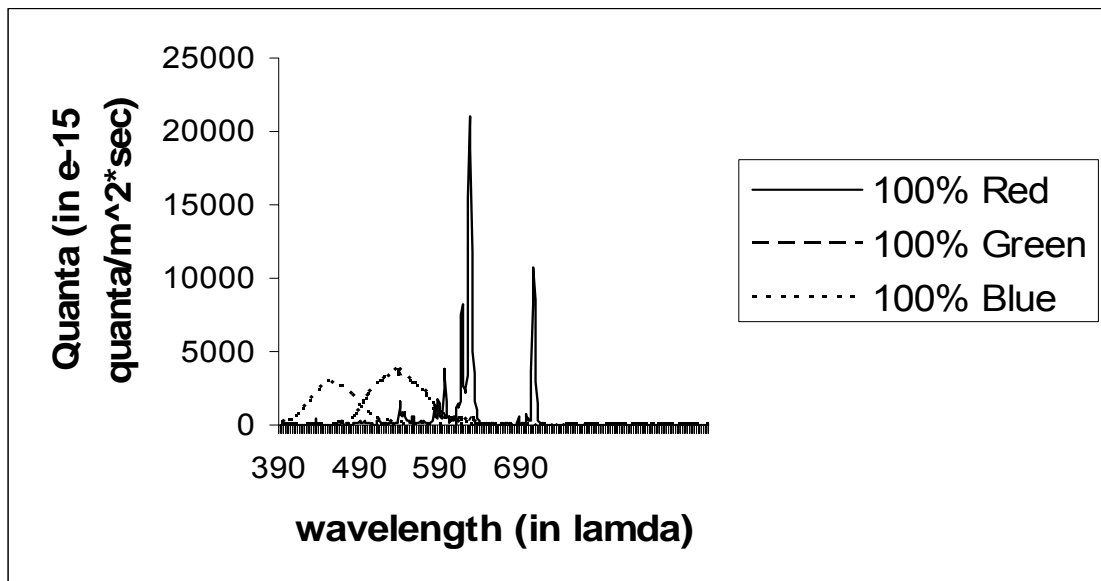


Figure 2. Quanta spectrum of the three phosphors.

2.2.2 Cone Fundamentals

The cone fundamentals describe the match of intensities of the three cone primaries to the wavelength of monochromatic test light of equal energy. In our study, we used the cone fundamentals of Stockman and Sharpe (1998; 1999; 2000).

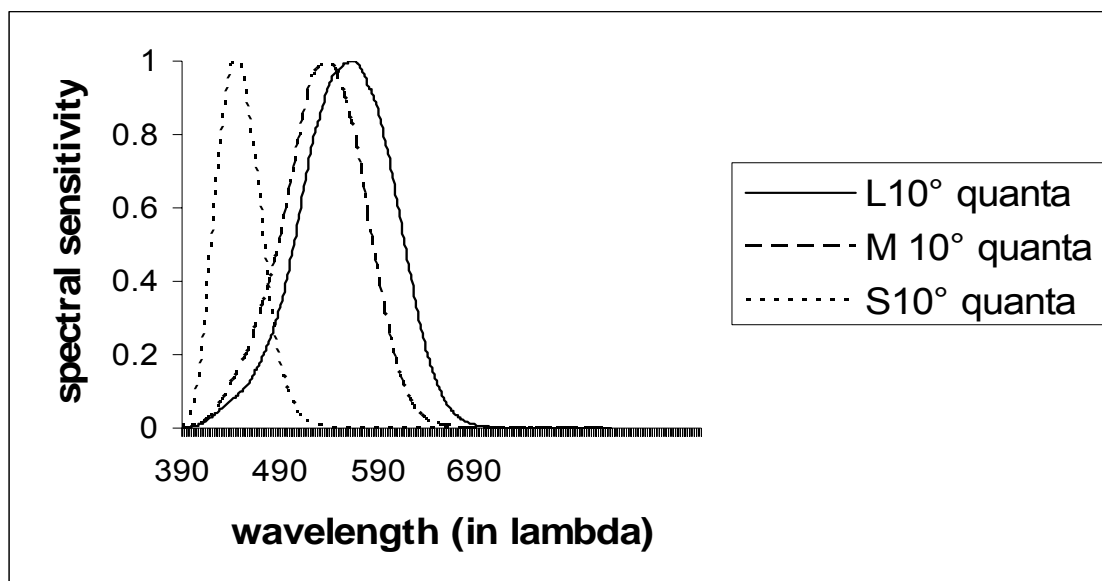


Figure 3. Cone fundamentals for 10°.

2.2.3 Silent Substitution (Estevez and Spekreijse 1982)

In the principle of trichromacy, any spectral light can be matched by a mixture of three fixed-color primary lights, noted as the primaries R, G, and B. Thus, the spectral test light U can be described as the addition of r units of primary R, g units of primary G and b units of primary B:

$$U = rR + gG + bB$$

The match is achieved when the amount of total quantal catch, which the three primaries produce in each of the three cone types, equals to the quantal catch produced by the spectral test light. This can be depicted in an equation as followed:

$$(rL_R + rM_R + rS_R) + (gL_G + gM_G + gS_G) + (bL_B + bM_B + bS_B) = rR + gG + bB$$

rL_R , rM_R , rS_R represent the effective quantal catch produced by the r units of primary R in the L-, M-, S-cone pigments (similarly gL_G , gM_G , gS_G by g units of primary G and bL_B , bM_B , bS_B by b units of primary B). Thus, the effective quantal catch produced in a single L-cone pigment by the spectral test light U is:

$$L = rL_R + gL_G + bL_B \quad (1)$$

Similarly, the effective quantal catch produced in a single M-cone pigment by the spectral test light U is:

$$M = rM_R + gM_G + bM_B \quad (2)$$

And the effective quantal catch produced in a single S-cone pigment by the spectral test light U is:

$$S = rS_R + gS_G + bS_B \quad (3)$$

These linear relations [equations (1), (2) and (3)] between the spectral test light $U = rR + gG + bB$ and the effective quantal catch produced in each cone pigment can be written in a matrix notation:

$$\begin{pmatrix} L \\ M \\ S \end{pmatrix} = \begin{bmatrix} L_R & L_G & L_B \\ M_R & M_G & M_B \\ S_R & S_G & S_B \end{bmatrix} * \begin{pmatrix} r \\ g \\ b \end{pmatrix} \quad (4)$$

The transformation from r, g, b values to L, M, S values can be represented as

$$LMS = LMS_rgb * rgb \quad (5)$$

The inverse of the transformation matrix LMS_rgb is written as

$$rgb = rgb_LMS * LMS \quad (6)$$

Each matrix coefficient expresses the effective quantal catch produced in each cone by each primary. Thus, for instance, the matrix coefficient L_G is calculated as:

$$L_G = \int L(\lambda) G(\lambda) d\lambda$$

$L(\lambda)$ represents the quantal spectral sensitivity of the L-cone pigment and $G(\lambda)$ the quantal spectral sensitivity of primary G. For each cone type, a test stimulus exists, which is equally effective for the other two cone types and thus only modulates this cone type, the so-called cone-isolating stimulus. The cone-isolating stimulus is proportional to the total effective quantal catch of its corresponding cone pigments. The spectral sensitivity functions, which relate the matching intensities of the three primary lights to the wavelength of this cone-isolating stimulus, are described in the cone fundamentals. In this study, each matrix coefficient was calculated by multiplying the Stockman and Sharpe cone fundamentals, determined for 10 degree and larger viewing conditions, with the emission spectra of the three phosphors and a constant k , and by integrating the product over wavelength. The constant k is different for each cone, depending on $\tau_{\lambda, \max}$, the product of the ocular media transmissivity and the absolute absorption coefficients for the wavelength of the maximal absorption probability for each cone. So k_L , k_M and k_S are derived from the multiplication of the foveal cone collecting area of $2.92 \mu\text{m}^2$ with a pupil's area of 50.26mm^2 and the factor $\tau_{\lambda, \max}$ of 0.6024, 0.555 and 0.1087 for the L-, M- and S-cones, and division of this product by 259.21mm^2 , since 16.1 mm is the distance between the nodal point of the lens and the retina (Wyszecki and Stiles 1982, Pugh 1988). Thus, the matrix coefficient allowed an estimate of the excitation of the cones by the phosphors:

$$\text{Matrix coefficient} = \int \text{cone fundamentals} * \text{emission spectra} * \text{constant } k \, d\lambda$$

Applying this formula to each of the nine matrix coefficients of LMS_rgb in equation (4) resulted in:

$$\begin{pmatrix} L \\ M \\ S \end{pmatrix} = \begin{bmatrix} 10396.25 & 19877.28 & 2795.86 \\ 3339.51 & 18342.24 & 4224.15 \\ 59.86 & 154.70 & 1903.71 \end{bmatrix} * \begin{pmatrix} r \\ g \\ b \end{pmatrix} \quad (7)$$

This led to the inverse matrix rgb_LMS

$$\begin{pmatrix} r \\ g \\ b \end{pmatrix} = \begin{bmatrix} 1.85e^{-4} & 2.02e^{-4} & 1.77e^{-4} \\ 3.30e^{-5} & 1.07e^{-4} & 1.55e^{-4} \\ 3.14e^{-6} & 1.08e^{-6} & 5.32e^{-4} \end{bmatrix} * \begin{pmatrix} L \\ M \\ S \end{pmatrix} \quad (8)$$

Each matrix coefficient of LMS_rgb represented the number of absorbed quanta per cone per second (quanta*cone⁻¹*s⁻¹), which an appropriate maximum phosphor intensity would have created, e.g. 100% red phosphor produced 10396.25 quanta*L-cone⁻¹*s⁻¹, 3339.51 quanta*M-cone⁻¹*s⁻¹ and 59.86 quanta*S-cone⁻¹*s⁻¹. Each inverse matrix coefficient of rgb_LMS held the unit of quanta*s*cone⁻¹ and allowed to calculate the appropriate intensity of the red, green and blue phosphors for any given quantal absorption in the cones.

2.2.4 L-cone Modulation for the mfVEP

When a stimulus is chosen to change the effective quantal catch produced in the three cones by ΔL, ΔM, ΔS, equation (6) can be altered as followed in order to calculate the corresponding values of Δr, Δg, Δb:

$$\begin{pmatrix} \Delta r \\ \Delta g \\ \Delta b \end{pmatrix} = \text{rgb_LMS} * \begin{pmatrix} \Delta L \\ \Delta M \\ \Delta S \end{pmatrix} \quad (9)$$

The so-called L-cone modulation is defined as an L-cone-isolating stimulus, which is equally effective for the M- and S-cones and thus only modulates the L-cones. In this study, the L-cone-isolating stimulus was a pattern-reversal stimulus alternating between red and green patches. Thus, for the L-cone modulation, the red and green patches produced the same quantal catch in the M-cones (ΔM = 0), and similarly the same number of quanta was absorbed in the S-cones (ΔS = 0). A maximal change of quantal catch in the L-cones (ΔL_{max}) could be obtained by setting the red phosphor at a maximum intensity of 100% (Δr = 1.0) [setting the green phosphor at maximum intensity (Δg = 1.0) required

$\Delta r > 1.0$ in order to meet the conditions ΔL_{\max} , $\Delta M = 0$ and $\Delta S = 0$; the blue phosphor is less significant in the stimulation of L-cones].

$$\begin{pmatrix} 1.0 \\ \Delta g \\ \Delta b \end{pmatrix} = \text{rgb_LMS} * \begin{pmatrix} \Delta L_{\max} \\ 0 \\ 0 \end{pmatrix} \quad (10)$$

Substitution of rgb_LMS by the inverse matrix coefficients in equation (8) resulted in:

$$\begin{aligned} 1.0 &= \Delta L_{\max} * (1.85e^{-4}) + 0 * (2.02e^{-4}) + 0 * (1.77e^{-4}) \\ \Delta g &= \Delta L_{\max} * (3.30e^{-5}) + 0 * (1.07e^{-4}) + 0 * (1.55e^{-4}) \\ \Delta b &= \Delta L_{\max} * (3.14e^{-6}) + 0 * (1.08e^{-6}) + 0 * (5.32e^{-4}) \end{aligned} \quad (11)$$

From equation (11), the following values were obtained for ΔL_{\max} , Δg and Δb :

$$\begin{aligned} \Delta L_{\max} &= 1.0 / (1.85e^{-4}) = 5405.41 \\ \Delta g &= 5405.41 * (3.30e^{-5}) = 0.1784 \\ \Delta b &= 5405.41 * (3.14e^{-6}) = 0.0170 \end{aligned}$$

$\Delta L_{\max} = 5405.41$ was the change of the quantal absorption, when the stimulus changed from red to green patch during the L-cone modulation, meaning one L-cone absorbed 5405.41 more quanta with the red patch than with the green one per second.

Δr , Δg , Δb corresponded to the phosphor's energy in %. To display colors accurately on the computer monitor, the input signal to the monitor (the voltage) had to be "gamma corrected". Most computer monitors have an intensity to voltage response curve, which is roughly a power function. This means that a pixel value in voltage sent to the monitor with an intensity of x , will actually be displayed as a pixel of an intensity equal to x^{gamma} on the monitor. Most monitors have a gamma between 1.7 and 2.7. Gamma correction is defined by applying the inverse of this function to the image before display, which can be

computed by $\text{new_pixel_value} = \text{old_pixel_value}^{(1.0/\text{gamma})}$. Here, the conversion of Δr , Δg , Δb into the Veris phosphor's energy scale, the scale of the operating device, reflected the gamma correction for the computer system, so that the output accurately reflected the image input (see 6.1 Screen Calibration Table):

Table 2. Veris scale for the calculated L-cone modulation

| phosphor | red | green | blue |
|-----------|-----|-------|------|
| red gun | 100 | 0 | 0 |
| green gun | 0 | 46 | 16 |

The red gun achieved maximal quantal absorption in the L-cones (ΔL_{max}), whereas the green gun produced minimal quantal absorption in the L-cones (ΔL_{min}).

2.2.4.1 L-cone Quantal Catch in the L-cone Modulation

As mentioned above, each matrix coefficient of LMS_rgb represented the number of absorbed quanta per cone per second, which an appropriate maximum phosphor intensity would have created. Derived from the above calculation, the L-cone modulation required the red phosphor being set at $\Delta r = 1.0$ (in % of phosphor's energy) for the red gun, while the green phosphor was set at $\Delta g = 0.1784$ and the blue phosphor at $\Delta b = 0.0170$ for the green gun.

$$\begin{pmatrix} \Delta L \\ \Delta M \\ \Delta S \end{pmatrix} = \text{LMS_rgb} * \begin{pmatrix} 1.0 \\ 0.1784 \\ 0.0170 \end{pmatrix} \quad (12)$$

Substitution of LMS_rgb by the transform matrix coefficients in equation (7) resulted in:

$$\begin{aligned} \Delta L &= 1.0 * 10396.25 + 0.1784 * 19877.28 + 0.0170 * 2795.86 \\ \Delta M &= 1.0 * 3339.51 + 0.1784 * 18342.24 + 0.0170 * 4224.15 \\ \Delta S &= 1.0 * 59.86 + 0.1784 * 154.70 + 0.0170 * 1903.71 \end{aligned} \quad (13)$$

Now, the L-cone quantal catch produced by each phosphor could be calculated via the first row in equation (13):

L-cone quantal catch produced by the

- red phosphor : $1.0 * 10396.25 = 10396.25 \text{ quanta} * \text{L-cone}^{-1} * \text{s}^{-1}$
- green phosphor: $0.1784 * 19877.28 = 3546.11 \text{ quanta} * \text{L-cone}^{-1} * \text{s}^{-1}$
- blue phosphor : $0.0170 * 2795.86 = 47.53 \text{ quanta} * \text{L-cone}^{-1} * \text{s}^{-1}$

The total L-cone quantal catch in the L-cone modulation summed up to

$$10396.25 + 3546.11 + 47.53 = 13989.89 \text{ quanta} * \text{L-cone}^{-1} * \text{s}^{-1}$$

2.2.4.2 M-cone Quantal Catch in the L-cone Modulation

The red gun with the ΔL_{\max} condition and the green gun with the ΔL_{\min} condition had to generate nearly the same M-cone quantal catch to confirm the correct calculation for the L-cone modulation. This is shown here through the calculations for the M-cone quantal catch via the second row of equation (13):

M-cone quantal catch produced by the

- red phosphor: $1.0 * 3339.51 = 3339.51 \text{ quanta} * \text{M-cone}^{-1} * \text{s}^{-1}$

The ΔL_{\max} condition produced an M-cone quantal catch of $3339.51 \text{ quanta} * \text{M-cone}^{-1} * \text{s}^{-1}$.

M-cone quantal catch produced by the

- green phosphor: $0.1784 * 18342.24 = 3272.26 \text{ quanta} * \text{M-cone}^{-1} * \text{s}^{-1}$
- blue phosphor: $0.0170 * 4224.15 = 71.81 \text{ quanta} * \text{M-cone}^{-1} * \text{s}^{-1}$
- green and blue phosphors:

$$3272.26 + 71.81 = 3344.07 \text{ quanta} * \text{M-cone}^{-1} * \text{s}^{-1}$$

The ΔL_{\min} condition produced an M-cone quantal catch of $3344.07 \text{ quanta} * \text{M-cone}^{-1} * \text{s}^{-1}$.

2.2.4.3 Cone Contrast for the L-cone Modulation

The modulation of the cone excitation could be quantified according to the cone contrast formula (Michaelson Contrast) with E_{\max} and E_{\min} representing the maximal and minimal cone excitations:

$$100\% * (E_{\max} - E_{\min}) / (E_{\max} + E_{\min}) \quad (14)$$

Thus, the calculated L-cone modulation had a maximal cone contrast of

$$100\% * [10396.25 - (3546.11 + 47.53)] / [10396.25 + (3546.11 + 47.53)] \\ = 48.63\%$$

for the L-cones, while the cone contrast for the M-cones and S-cones was maintained at 0 %.

Our calculations confirmed the nearly equal quantal absorptions in the M-cones for the ΔL_{\max} and ΔL_{\min} conditions. However so far, these calculations were relied on accurate calibration measurements as a prerequisite. In order to avoid the influence of calibration errors arose from the susceptibility of the spectroradiometer to interferences, the L-cone-isolating setting was adjusted in contrast and intensity to pre-studied calibration series obtained in Tübingen, Germany (see Albrecht et al. 2002), and to the recordings from a protanope. By these adjustments, a precise silent substitution was reached by an L-cone-isolating setting of 50% cone contrast, named L50, which was used in this study.

Table 3. Veris scale for the L50 setting

| phosphor | red | green | blue |
|-----------|-----|-------|------|
| red gun | 98 | 9 | 4 |
| green gun | 37 | 33 | 1 |

Reducing the cone contrast in the L50 setting by half yielded an L-cone-isolating setting with 25% cone contrast, here named as the L25 setting:

Table 4. Veris scale for the L25 setting

| phosphor | red | green | blue |
|-----------|-----|-------|------|
| red gun | 88 | 19 | 3 |
| green gun | 60 | 30 | 2 |

2.2.5 M-cone Modulation for the mfVEP

In this study, the M-cone-isolating stimulus, the so-called M-cone modulation, was a pattern-reversal stimulus alternating between green and red patches. In analogy to the L-cone modulation, the green and red patches of the M-cone modulation evoked the same quantal catch in the L-cones ($\Delta L = 0$), as well as in the S-cones ($\Delta S = 0$). A maximal change of quantal catch in the M-cones (ΔM_{\max}) was also obtained by setting the red phosphor at a maximum intensity of 100% ($\Delta r = 1.0$) [setting the green phosphor at maximum intensity ($\Delta g = 1.0$) required $\Delta r > 1.0$ in order to meet the conditions ΔM_{\max} , $\Delta L = 0$ and $\Delta S = 0$; the blue phosphor is also less significant in the stimulation of M-cones].

$$\begin{pmatrix} 1.0 \\ \Delta g \\ \Delta b \end{pmatrix} = \text{rgb_LMS} * \begin{pmatrix} 0 \\ \Delta M_{\max} \\ 0 \end{pmatrix} \quad (15)$$

Substitution of `rgb_LMS` by the inverse matrix coefficients in equation (8) resulted in:

$$\begin{aligned} 1.0 &= 0 * (1.85e^{-4}) + \Delta M_{\max} * (2.02e^{-4}) + 0 * (1.77e^{-4}) \\ \Delta g &= 0 * (3.30e^{-5}) + \Delta M_{\max} * (1.07e^{-4}) + 0 * (1.55e^{-4}) \\ \Delta b &= 0 * (3.14e^{-6}) + \Delta M_{\max} * (1.08e^{-6}) + 0 * (5.32e^{-4}) \end{aligned} \quad (16)$$

From equation (16), the following values were obtained for ΔM_{\max} , Δg and Δb :

$$\begin{aligned} \Delta M_{\max} &= 1.0 / (2.02e^{-4}) = 4950.50 \\ \Delta g &= 4950.50 * (1.07e^{-4}) = 0.5297 \\ \Delta b &= 4950.50 * (1.08e^{-6}) = 0.0053 \end{aligned}$$

Δr , Δg , Δb corresponded to the phosphor's energy in % and were converted into the Veris scale, in accordance with the gamma correction for the computer system (see 6.1 Screen Calibration Table):

Table 5. Veris scale for calculated M-cone modulation

| phosphor | red | green | blue |
|-----------|-----|-------|------|
| green gun | 0 | 75 | 0 |
| red gun | 100 | 0 | 9 |

The green gun achieved maximal quantal absorption in the M-cones (ΔM_{\max}), whereas the red gun produced minimal quantal absorption in the M-cones (ΔM_{\min}).

2.2.5.1 M-cone Quantal Catch in the M-cone Modulation

In the M-cone modulation, the green phosphor was set at $\Delta g = 0.5297$ (in % phosphor's energy) for the green gun, and the red phosphor was set at $\Delta r = 1.0$ and the blue phosphor at $\Delta b = 0.0053$ for the red gun.

$$\begin{pmatrix} \Delta L \\ \Delta M \\ \Delta S \end{pmatrix} = \text{LMS_rgb} * \begin{pmatrix} 1 \\ 0.5297 \\ 0.0053 \end{pmatrix} \quad (17)$$

Substitution of LMS_rgb by the transform matrix coefficients in equation (7) resulted in:

$$\begin{aligned} \Delta L &= 1.0 * 10396.25 + 0.5297 * 19877.28 + 0.0053 * 2795.86 \\ \Delta M &= 1.0 * 3339.51 + 0.5297 * 18342.24 + 0.0053 * 4224.15 \\ \Delta S &= 1.0 * 59.86 + 0.5297 * 154.70 + 0.0053 * 1903.71 \end{aligned} \quad (18)$$

Now, the M-cone quantal catch produced by each phosphor could be calculated via the second row of equation (18):

M-cone quantal catch produced by the

- green phosphor: $0.5297 * 18342.24 = 9715.88 \text{ quanta} * \text{M-cone}^{-1} * \text{s}^{-1}$
- red phosphor : $1.0 * 3339.51 = 3339.51 \text{ quanta} * \text{M-cone}^{-1} * \text{s}^{-1}$
- blue phosphor : $0.0053 * 4224.15 = 22.39 \text{ quanta} * \text{M-cone}^{-1} * \text{s}^{-1}$

The total M-cone quantal catch in the M-cone modulation summed up to

$$3339.51 + 9715.88 + 22.39 = 13077.78 \text{ quanta} * \text{M-cone}^{-1} * \text{s}^{-1}$$

2.2.5.2 L-cone Quantal Catch in the M-cone Modulation

The green gun with the ΔM_{\max} condition and the red gun with the ΔM_{\min} condition had to generate nearly the same L-cone quantal catch to confirm the correct calculation for the M-cone modulation. This is shown here through the calculations of the L-cone quantal catch via the first row of equation (18):

L-cone quantal catch produced by the

- green phosphor: $0.5297 * 19877.28 = 10529.0 \text{ quanta} * \text{L-cone}^{-1} * \text{s}^{-1}$

The ΔM_{\max} condition produced an L-cone quantal catch of $10529.0 \text{ quanta} * \text{L-cone}^{-1} * \text{s}^{-1}$.

L-cone quantal catch produced by the

- red phosphor: $1.0 * 10396.25 = 10396.25 \text{ quanta} * \text{L-cone}^{-1} * \text{s}^{-1}$
- blue phosphor: $0.0053 * 2795.86 = 14.82 \text{ quanta} * \text{L-cone}^{-1} * \text{s}^{-1}$
- red and blue phosphors:

$$10396.25 + 14.82 = 10411.07 \text{ quanta} * \text{L-cone}^{-1} * \text{s}^{-1}$$

The ΔM_{\min} condition produced an L-cone quantal catch of $10411.07 \text{ quanta} * \text{L-cone}^{-1} * \text{s}^{-1}$.

2.2.5.3 Cone Contrast for the M-cone Modulation

According to equation (14), the calculated M-cone modulation should had a maximal cone contrast of

$$100\% * [9715.88 - (3339.51 + 22.39)] / [9715.88 + (3339.51 + 22.39)] = 48.59\%$$

for the M-cones, while the cone contrast for the L-cones and S-cones was maintained at 0 %.

Similarly as described above for the L-cone modulation, the M-cone-isolating setting was adjusted in contrast and intensity to pre-studied calibration series obtained in Tübingen, Germany (see Albrecht et al. 2002), and to the recordings from a deuteranope. By these adjustments, a precise silent substitution was reached by an M-cone-isolating setting of 50% cone contrast, named M50, which was used in this study.

Table 6. Veris scale for the M50 setting

| phosphor | red | green | blue |
|-----------|-----|-------|------|
| green gun | 10 | 71 | 3 |
| red gun | 100 | 7 | 34 |

Reducing the cone contrast in the M50 setting by half yielded an M-cone-isolating setting with 25% cone contrast, here named as the M25 setting:

Table 7. Veris scale for the M25 setting

| phosphor | red | green | blue |
|-----------|-----|-------|------|
| green gun | 54 | 63 | 18 |
| red gun | 88 | 38 | 30 |

2.3 L- and M-cone Isolation for the mfERG

The calibration of the mfERG monitor was performed by the same compact array spectroradiometer (CAS 140, Instrument Systems, München, Germany), yielding an emission spectra with a primary peak at 627 nm and a secondary peak at 707 nm for the red phosphor, an emission spectra peaking at 522 nm for the green phosphor and an emission spectra peaking at 453 nm for the blue

phosphor of the monitor. The maximum intensities of the red, green, and blue phosphors were 24, 79.3, and 13.8 cd/m², respectively. The L- and M-cone isolations used for the mfERG recordings were generated analogous to the L- and M-cone isolations for the mfVEP as described in 2.2. (for details see Albrecht et al. 2002).

2.4 Multifocal Visual Evoked Potential (mfVEP)

2.4.1 Hardware and Software

The multifocal visual evoked potentials (mfVEPs) were recorded with the Visual Evoked Response Imaging System (VERIS) Science 4.2beta915 featured by the EDI (Electro Diagnostic Imaging, Inc., San Mateo, CA) (Sutter and Tran 1992). The VERIS Science 4.2beta915 is an electrophysiological recording system, used as a steering device for the integrated management of information and instruments.

The VERIS software was executed under the Macintosh OS 7.5 (Windows) Operating System. The stimulus was generated on a 21 inch Apple Studio Display Monitor (Apple Computer, Inc., Cupertino, CA) driven at a frame rate of 75 Hz. The resolution of the monitor was set at 1024 x 768 pixels, and the checks inside the smallest sector had an average of approximately 20 pixels. The specific stimulator parameters were adjusted as followed in the VERIS 4.2 Setting:

Table 8. Stimulator parameters in the Veris 4.2 setting

| | | | |
|------------|-------------------------|---------------------------|---------|
| GEOMETRY | Screen | distance: | 34 cm |
| | | height: | 28.3 cm |
| | | width: | 38 cm |
| | Fixation | cross | |
| | | diameter: | 3° |
| | | pen size: | 9 |
| | | fixation x: | 0 |
| | | fixation y: | 0 |
| | Stimulus Picture: | Dartboard 60 With Pattern | |
| COLORS | frame per m-step: | 1 | |
| | show sub Pattern Colors | | |
| TEMPORAL | frame rate: | 75.0322827 Hz | |
| | M-sequence exponent: | 15 | |
| | frames per m-step: | 1 | |
| | max kernel order: | 3 | |
| | max kernel spread: | 4 | |
| | memory | < 319 ms | |
| | no. of segments: | 16 | |
| | samples per frame: | 16 | |
| | pre-exposure: | 1000 ms | |
| AQUISITION | board type: | PCI | |
| | analogue channels: | 3 | |
| | board gain: | 1 | |
| | gain: | 100 K | |
| | low cutoff: | 3 Hz | |
| | high cutoff: | 100 Hz | |
| | notch filter: | out | |
| | no camera | | |

2.4.2 Multifocal Stimulation in the mfVEP

The mfVEP stimulus picture was depicted in a dartboard array consisting of 60 sectors (Dart Board 60 With Pattern). Each of the 60 sectors contained a checkerboard pattern made up by 16 checks, which were displayed in a color-alternated 4 x 4 arrangement. The entire display spanned a circular central visual field of 22.2° radius. The visual angle α in (°) for the visual field was calculated according to the formula

$$\tan \alpha = \frac{w}{2xd}$$

with w representing the width of the visual field (mm) and d the distance of pattern from the corneal surface (mm). The central 4 sectors fell within 1.2° (i.e. a diameter of 2.4°) of the foveal center, the 20 sectors of the next two rings within 5.8° and the 36 sectors of the next three rings within the 22.2°. A black fixation cross was displayed at the center of the stimulus picture. The sectors were scaled with eccentricity according to cortical magnification in human striate cortex (V1), so that each sector activates nearly equal area of the visual cortex. Thus, each stimulus produces approximately equal amplitude in focal response and improves the signal-to-noise ratio at each location. However, since inter-subject variation in cortical folding are preserved, the sectors may still happen to activate more than one retinotopic locus of the visual cortex. Therefore even amplitudes from scaled stimuli can differ due to opposed signal orientation or ultimately signal cancellation (Baseler et al. 1994).

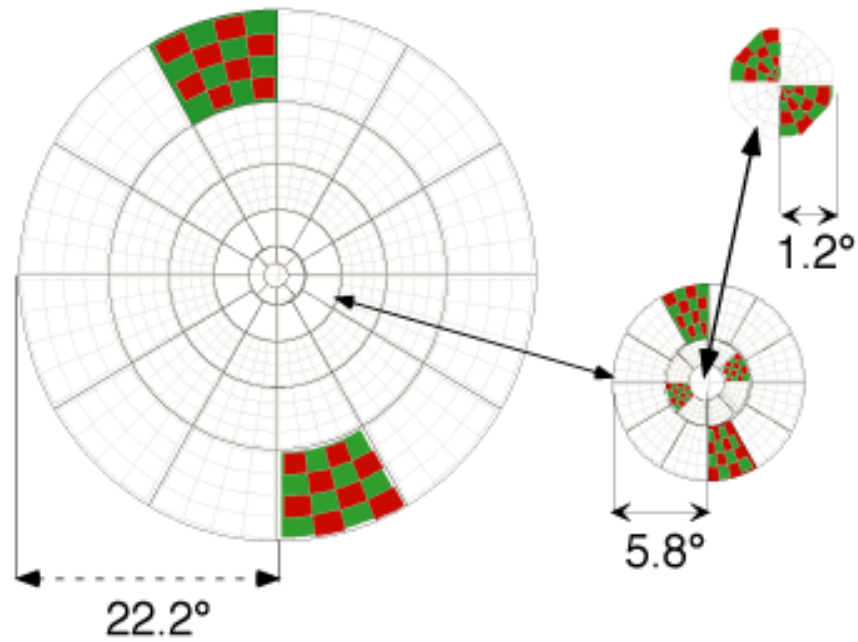


Figure 4. The stimulus array for the mfVEP recordings.

The mfVEP stimulus was used as a pattern-reversal stimulus, as the 16 element checkerboard of each sector abruptly alternated between two states. Both states had a probability of 0.5 at any frame change to alternate in color between two values, which were carefully selected so as to modulate activity in a single cone class. As the display monitor was set at a frame rate of 75 Hz, the frame here re-drew every 13.3 ms. During the recording, each sector of the array appeared to flicker randomly. In truth, each sector was stimulated sequentially in a specific order, a pseudo-random cyclical series of +1s and -1s, called the m-sequence. These binary digits +1 and -1 represent the two possible reversal states and are named the m-sequence steps. In this study, one frame per m-step was chosen, consequently one m-sequence step lasted 13.3 ms consistent with the frame change. During one run of recording, the sectors went through one m-sequence. The m-sequence exponent was set at 15, meaning that there were $(2^{15} - 1)$ m-steps per m-sequence, so that the total recording time lasted $[(2^{15} - 1) * 13.3 \text{ ms}] = 7.2633517 \text{ mins}$. The temporal modulation of each sector followed the same m-sequence but started at a different point along the m-sequence cycle. Therefore there was a time lapse between the modulation of consecutive sectors ensuring their independent

uncorrelated stimulation. This allowed an extraction of the individual contributions of the 60 locations from a continuous EEG signal, which was recorded from each bipolar response channel. Thus, the mfVEP final data were displayed as 60 individual traces spatially arranged according to the stimulus array. In this study, the first slice of the second order kernel were extracted for each stimulus patch using Veris Science 4.2beta915 software from EDI. All other analyses were done with programs written in MATLAB (Mathworks, Natick, MA).

2.4.3 mfVEP Stimulus Calibration

The screen was set at the time average mean luminance, which was 16.8 and 30.6 cd/m^2 for the L- and M-cone modulations. The percent contrast was set at 50% for the L- and M-cone modulations. The percent contrast is defined by the Michaelson formula:

$$\text{Michaelson contrast [\%]} = [(L_{\text{max}} - L_{\text{min}})/(L_{\text{max}} + L_{\text{min}})] \times 100$$

L_{max} and L_{min} are the maximal and minimal luminances of the pattern elements. They were measured by a spot photometer.

2.4.4 Electrode Placement and Three Channels

Multifocal VEPs were recorded on three channels with 4 gold cup electrodes placed on the occipital scalp in the following arrangement:

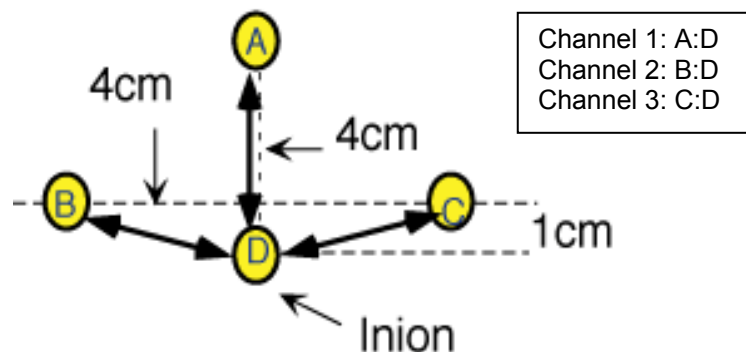


Figure 5. Electrode positions and configurations for the three channels of recording.

Electrode A was placed 4 cm above the inion, electrodes B and C were placed 1 cm above and 4 cm lateral to the inion on both sides. All three electrodes A, B, and C were each referenced to electrode D placed at the inion. The associated differential signals were recorded on three separate channels as indicated in Figure 5. A forehead electrode served as the ground electrode. All responses in the figures are displayed with the reference (inion) electrode as negative. The scalp-electrode impedance was kept below 5 kOhms for all three channels to achieve recordings as noise-free as possible.

2.4.5 mfVEP Recording Parameters

Analogue low- and high-frequency cutoff filters were set at 3 and 100 Hz (1/2 amplitude; Grass preamplifier P511J, Quincy, Mass.). The notch filter was turned off. The continuous mfVEP signals were amplified and were sampled at a rate of 1200 Hz (every 0.83 ms). Three 7-min runs of mfVEP recordings were performed and then averaged in order to increase the signal-to-noise ratio between the mfVEP and the background noise.

2.4.6 mfVEP Recording Protocol

The mfVEP study was conducted in the Psychology Department of Columbia University in New York, U.S.A.. Color vision was tested with the pseudoisochromatic plates and the Nagel anomaloscope. After ensuring a normal color vision, the subjects were hooked up for the mfVEP recordings in a relaxing position to minimize muscle and other artifact.

First of all, the inion at the occipital scalp of each subject was found as a landmark for the electrode placement scheme depicted in Figure 5. All four electrode sites on scalp were marked with a green pen. The skin areas for electrode placement on the forehead and on the occipital scalp were cleaned with single-used electrode skin preparation pads (saturated with 70% Isopropyl Alcohol and Pumice). To further ensure a low resistance, an abrasive skin prepping gel (Nuprep[®]) was lightly rubbed into the cleaned electrode sites on the scalp. The gold electrodes were submerged with conducting electrode paste (Genuine Grass EC2 Electrode Cream[®] by Grass Instrument Division/Astro-

med, Inc., W. Warwick, RI 02893) and then applied to the clean electrode sites. Electrodes were held in place by self-adherent wrap. After finishing the electrode placements, the subject was comfortably sat in front of the display monitor at a distance of 34 cm. None of both eyes were dilated. One eye was patched up with a light-tight opaque patch in order to conduct monocular mfVEP recordings. The subject was asked to fixate at the 'X' in the center of the stimulus and to refrain from moving, talking or swallowing during the runs.

All recordings to L- and M-cone modulations for each subject, which are compared in the result section (see 3.2 mfVEP Studies), were conducted in a single session, under identical electrode placements and amplification conditions but with a random assignment of orders. In this single session, each L- and M-cone modulation for each subject was repeated in three 7-min runs, e.g. for DH's results in Figure 13, three runs to 50% L-cone modulation and three runs to 50% M-cone modulation were recorded in random order in a single session; for DH's results in Figure 17, three runs to 25% L-cone modulation and three runs to 25% M-cone modulation were recorded in random order in a single session; for DH's results in Figure 18, three runs to 25% L-cone modulation and three runs to 50% M-cone modulation were recorded in random order in a single session; etc. For the ease of the subject, each run was divided into 16 overlapping segments, each lasting 27.26 s. Each run lasted approximately 7.26 mins.

2.5 Multifocal Electroretinogram (mfERG)

2.5.1 Hardware and Software

The multifocal electroretinograms (mfERGs) were recorded with the VERIS system software (Version 3.0.1) from EDI (Sutter and Tran 1992). The stimulus was generated on a flat-screen SONY Trinitron monitor driven at a frame rate of 75 Hz. The resolution of the monitor was set at 1024 x 768 pixels.

2.5.2 Multifocal Stimulation in the mfERG

The mfERG stimulus picture consisted of 103 hexagonal elements, which were scaled with eccentricity in accordance with the variations in cone density, so that approximately equal amplitude was produced for each hexagon. The stimulus picture spanned a width of 32 cm and a height of 27.5 cm and was presented at a distance of 18 cm. Thus, the entire display subtended $84^\circ \times 75^\circ$ of visual angle.

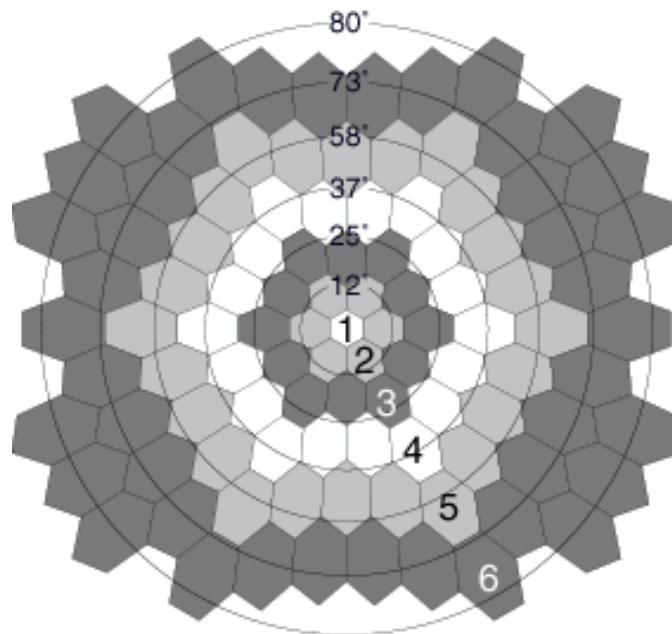


Figure 6. The stimulus array for the mfERG recordings. The numbers indicate the six concentric rings used to analyse the summed signals.

Sutter and Tran (1992) were the first, who used the technique of simultaneous ERG recordings with an independent uncorrelated stimulation of small retinal areas in order to obtain ERG response topography maps. They selected the pseudo-random m-sequence as a sequential temporal modulation of the individual sectors, which allowed them to assign each response to a certain timing. By cross-correlation between the m-sequence and the contiguous response cycle, the local response contributions, identified by its timing dimension, could be extracted. In this study, the mfERG hexagons were sequentially reversed in color according to a pseudo-random m-sequence,

which included a total of $2^{14} - 1$ elements. This corresponded to a total recording time of 3 mins and 38.5 s for each run.

The traces produced by multifocal stimulation were analysed in binary kernels (Sutter 2000). The first-order kernel is a linear approximation of the total response, which is calculated by addition of all records following the presentation of a flash in that patch (e.g. the presentation of a white patch), and subtraction of all records following a dark frame (equal to a 'non-presentation'). In this way, the flash response to the patch is built up, while all responses, which do not contribute to the flash response, are eliminated. The second-order kernel measures the influence of preceding flashes on the flash response to that patch. The first slice of the second-order kernel measures the effect of an immediately preceding flash, the second slice of the second-order kernel the effect of the flash two frames away, and so forth. First-order kernel responses were taken for analysis with the VERIS system software (Version 3.0.1) from EDI. For mfERG recordings, the first-order kernel corresponds to the linear responses in the outer and middle retinal layer including the photoreceptors (Hood et al. 1997), whereas the second-order kernel reflects the non-linear activity of the inner retinal layer and thus of the ganglion cells, the so-called optic nerve head component (ONHC) (Sutter and Bearse 1999; Sutter et al., 1999).

2.5.3 mfERG Stimulus Calibration

The screen was set at the time average mean luminance, which was 19.2 and 33.8 cd/m^2 for the L- and M-cone modulation. The percent contrast was set at 50% for the L- and M-cone modulation. The ambient room illumination was maintained at 150 cd/m^2 in order to suppress the rod inputs.

2.5.4 mfERG Electrodes

Multifocal ERGs were registered by DTL-electrodes (named by Dawson, Trick and Litzkow 1979) and applied at the limb of the lower lid of the eye. A DTL-electrode is made up of 50 μm drilled with silver laminated Nylon fibers coiled round a plug. The free end of the Nylon fibers is attached at the nose,

whilst the coiled up end is connected to the amplifier. Since the fibers are very fine and thus flexible, the DTL-electrodes can adapt to any corneal form, which also contributes to the patients' comfort. The fibers are only fixed by adhesion to the bulbi oculi. In this way, they can potentially be used for several hours without causing any damages to the eye. To maintain a good registration quality and for hygienic reasons, the DTL-electrodes are only for one single use. Compared to contact lenses electrodes, however, the amplitudes registered by DTL-electrodes are up to 10% smaller as reported by Dawson et al. (1982). Additionally, they are also less resistant to blinking of the eyes. However, even a delicate change in the position of the electrode can be noticed at the oscilloscope and can then immediately be corrected.

2.5.5 mfERG Recording Parameters

The continuous mfERG recordings were amplified by 200 K, with the low- and high-frequency cutoffs set at 10 and 100 Hz for half amplitude (Grass Instruments), and were sampled at 1200 Hz (every 0.83 ms). Electrode resistance of the reference electrode was kept below 5 kOhms.

2.5.6 mfERG Recording Protocol

For two subjects, AY and DH, mfERG recordings were conducted in the Division of Experimental Ophthalmology, University Eye Hospital of the University of Tübingen in Germany.

First of all, the pupil of the tested eye was dilated (around 8 mm) with a mydriatic (0.5% tropicamide). After maximal dilation of the pupil, the skin areas for electrode placement were cleaned with single-used alcohol swabs. The reference electrode was positioned near the orbital rim temporally, whereas the ground skin electrode was placed on the forehead. The gold skin electrodes were submerged with electrode paste (Elefix EEG paste[®] by Nihon Kohden America, Inc., Foothill Ranch, CA 92610), applied to the clean electrode sites and attached with some adhesive tape. The subject's eye was then fitted with a DTL-fiber electrode and kept light-adapted before and during the mfERG recordings. After finishing the electrode placement, the subject was comfortably

sat in front of the flat-screen monitor at a distance of 18 cm. The subject was asked to fixate at the center of the stimulus and to refrain from blinking during the runs.

The L- and M-cone-isolating recordings for each subject were performed in a single run, under identical electrode placement and amplification conditions but with a random assignment of orders to make the results comparable. To improve the subject's ability to maintain fixation and to prevent blinking during the recording time, each run was divided into 16 overlapping segments, each lasting 13.65 s. Therefore each run lasted 3 mins and 38.5 s.

3 Results

3.1 Test Studies for the L- and M-cone Modulation Settings

3.1.1 Dichromat Data

As mentioned in the method section, the calculated mfVEP settings were adjusted to pre-studied calibration series obtained in Tübingen, Germany (see Albrecht et al. 2002) and to the recordings from a protanope and deuteranope. Precise silent substitution was confirmed by the dichromats' recordings at the adjusted L50 and M50 settings, where they showed no residual cone response. In addition to that, both the initially calculated L- and M-cone modulations and the adjusted L50 and M50 settings were tested on two subjects (DH and AY). The calculated setting and the adjusted setting for both the L- and for the M-cone modulation produced similar mfVEP amplitudes with no significant differences.

3.1.2 Cone Fundamentals for 2°

In another reliability test study, the L- and M-cone modulations were calculated the same way as described in the method section (see 2.2 L- and M-cone Isolation for the mfVEP), with the exception that this time the cone fundamentals for 2° viewing conditions (Stockman and Sharpe 2000) were used instead of the cone fundamentals for the 10° or larger viewing conditions (see 2.2.2 Cone Fundamentals). Their results showed that an adjustment of the settings by using the 2° fundamentals would change the cone contrast values by less than 1.5 %, the phosphor settings by about 1% and the linearized gun values by about 2%. These minimal changes are insignificant in terms of the mfVEP amplitudes and their variability, as they lie within the error of measurement.

3.2 mfVEP Studies

3.2.1 General Features of VEP Responses

As previously mentioned, there is a great inter-subject variability in all mfVEP responses due to the position of the calcarine sulcus relative to the external landmarks (e.g. inion) and to the different foldings of the cortex among individuals. As the reference electrode was placed at the inion, which should approximately correspond to the calcarine sulcus, the responses to stimulation of the upper and lower visual field in channel 1 are reversed in polarity (upper field projects to lower bank of calcarine and lower field projects to upper bank of calcarine) (Baseler et al. 1994; Hood and Zhang 2000).

In this study, multifocal stimulation with a pattern-reversal stimulus was conducted, which elicited VEP signals each consisting of a negative component at an implicit time of 75 ms (N75), a positive component at an implicit time of 100 ms (P100), followed by a negative component at an implicit time of 135 ms (N135). Amplitude measurements were made between peaks and troughs of the deflections. Implicit times were taken from the onset of the stimulus to the peak of the component concerned (Harding et al. 1996). The polarity of the peaks can vary across the hemi-fields due to variations in the folding of local regions of the cortex.

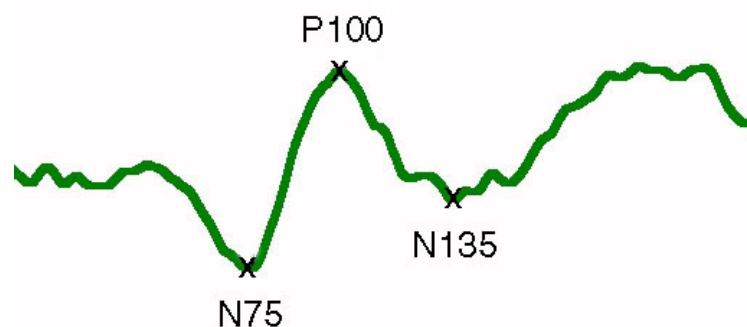


Figure 7. A single VEP signal to pattern-reversal.

3.2.2 Displaying the mfVEP Responses

The standard display of the 60 individual mfVEP responses is spatially arranged, but not scaled, according to the stimulus dartboard. To compare the L-cone to the M-cone modulation, which are depicted as red and green records, both records were overlaid on each other. The records, presented in the figures below, are the averages of three 7-min runs of mfVEP recordings.

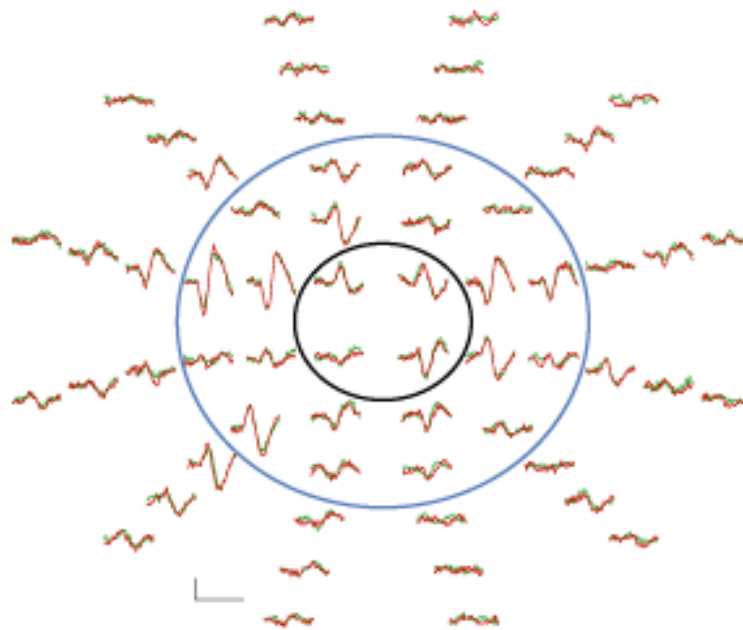


Figure 8. The 60 mfVEP responses of subject AY to the L-cone (red traces) and M-cone (green traces) modulations at 50% contrast condition from channel 1. The calibration bars indicate 200 nV and 200 ms.

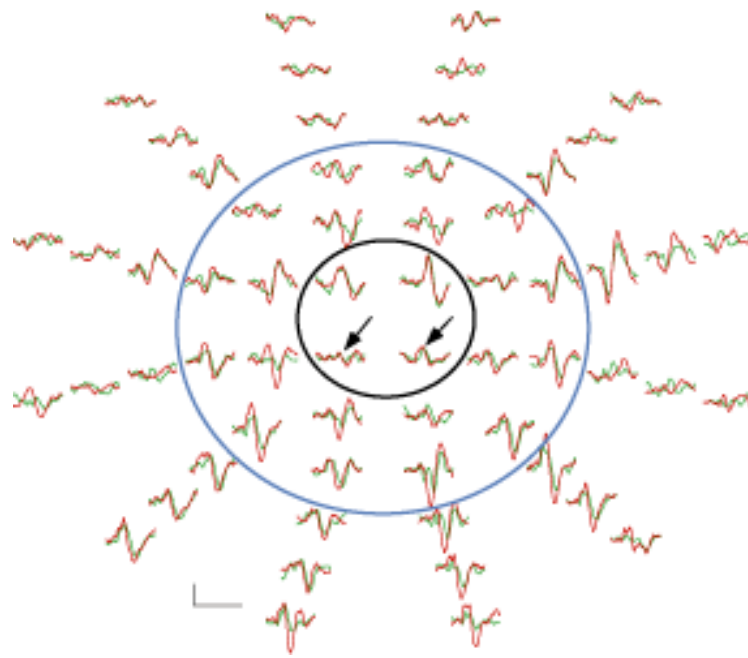


Figure 9. mfVEP responses to 50% contrast condition from channel 1 for subject DH. The calibration bars indicate 200 nV and 200 ms.

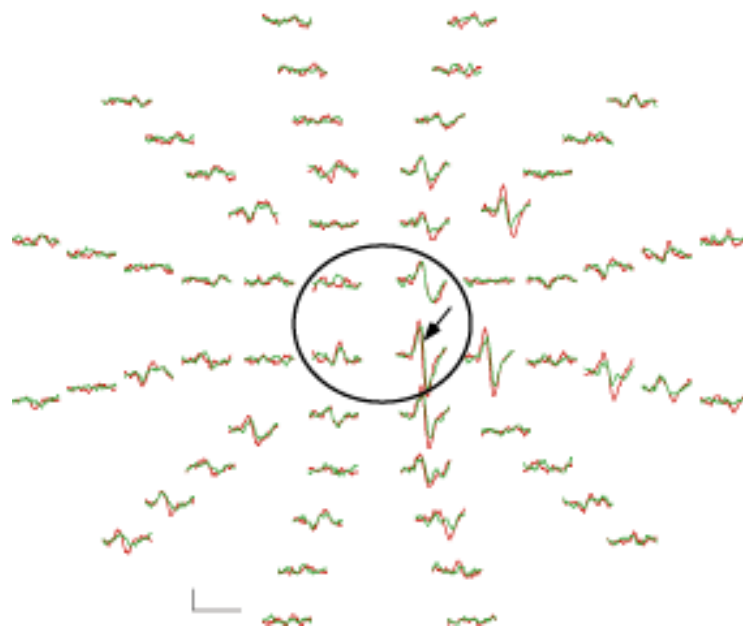


Figure 10. mfVEP responses to 50% contrast condition from channel 2 for subject DH. The calibration bars indicate 200 nV and 200 ms.

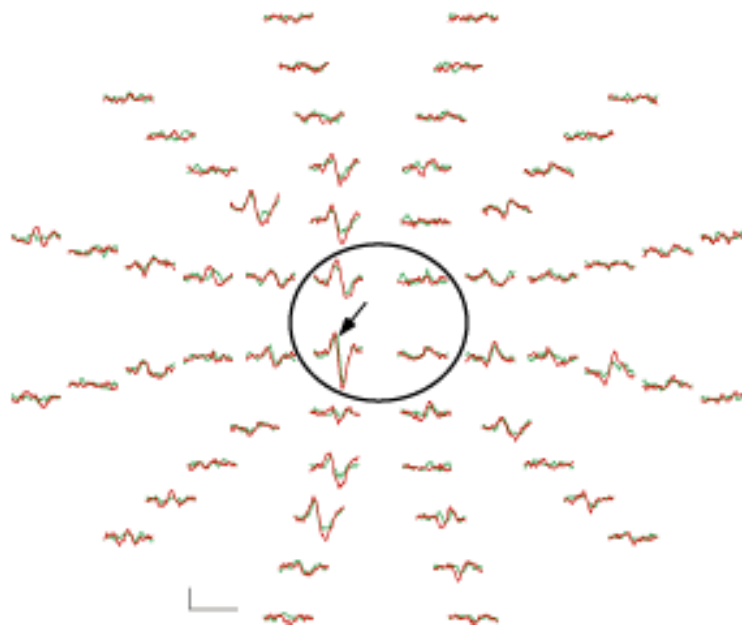


Figure 11. mfVEP responses to 50% contrast condition from channel 3 for subject DH. The calibration bars indicate 200 nV and 200 ms.

The primary interest of recording comes from channel 1, which provides the largest bipolar recordings of all channels, since the vertical line of its electrode positions was meant to be perpendicular to the calcarine sulcus. However, in reality, a line drawn through the calcarine sulcus often intersects the skin at a point lower than theinion, which explains the often larger responses in the lower fields (Hood and Zhang 2000).

Channel 2 and 3 were added in order to obtain a better signal-to-noise ratio and thus to distinguish the usually small mfVEP responses from the background noise. Especially the recordings to stimulation of the central visual field are often larger with laterally placed electrodes (Klistorner and Graham 2000; Hood et al. 2002b). This is illustrated by two of the central responses, indicated by the arrows in Figures 10 and 11, which are clearly larger than the corresponding responses from channel 1, indicated by the arrows in Figure 9.

3.2.3 Grouping of the mfVEP Responses

In this study, the individual mfVEP responses, as depicted in Figure 8 to 11, were grouped as shown in Figure 12 and then summed in order to increase the signal-to-noise ratio and better display the differences among individuals.

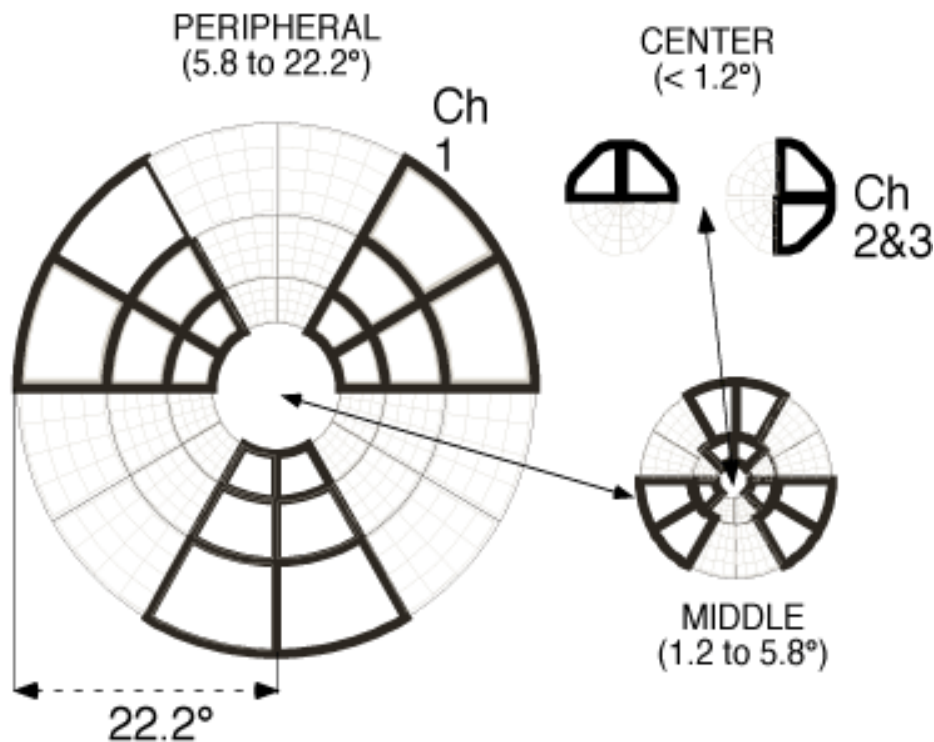


Figure 12. Grouping of the mfVEP responses. The mfVEP responses were grouped into 6 peripheral (5.8° to 22.2°), 6 middle (1.2° to 5.8°) and 2 central (<1.2°) groups and summed within the groups.

In particular, the 36 sectors of the three most peripheral rings, falling between 5.8° and 22.2°, were divided into six groups of six sectors and their responses summed. Further, the 20 sectors of the middle two rings, falling between 5.8° and 1.2°, were divided into two groups of four sectors and four groups of three sectors and their responses summed. Finally, for the central ring, the upper two and the lower two sectors were grouped in the case of channel 1, and the left and right two sectors were grouped in the cases of channels 2 and 3, and their responses summed. As in previous studies (Klistorner and Graham 1999; Hood et al. 2000a; Hood and Zhang 2000), this way of grouping is meant to sum up

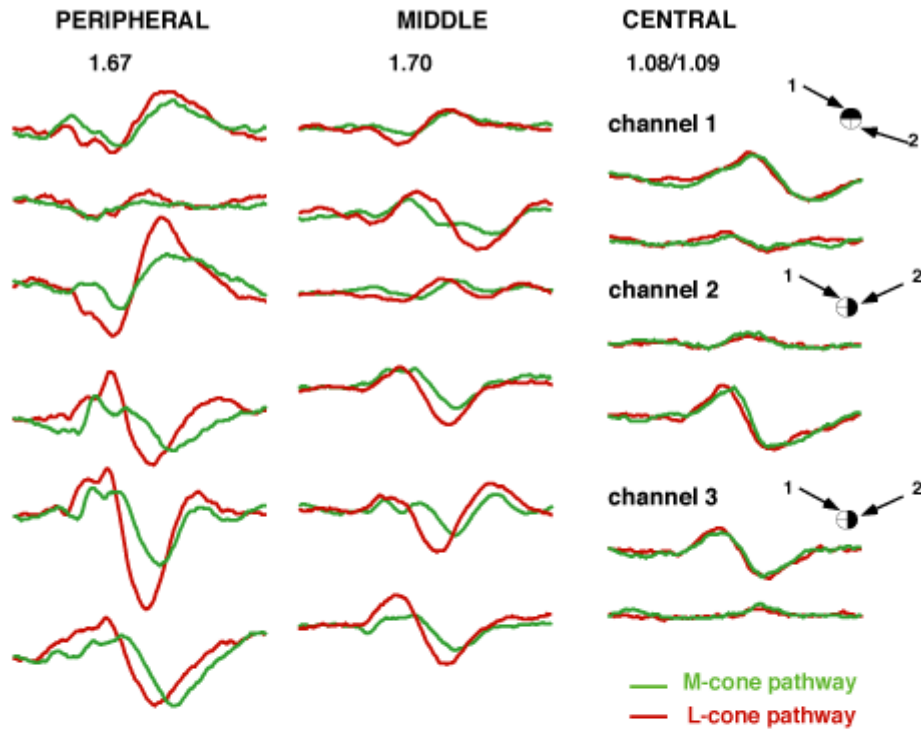
only responses of similar waveforms. In channel 1, the polarity of N75 tends to be positive in the lower field, and negative in the upper field, whereas in channel 2 and 3, they are usually reversed in polarity as the vertical midline is crossed. Thus, the central responses, which are a main focus of this study, and the responses from the midline are known to differ in waveform from other responses and therefore are displayed in separate groups.

3.2.4 Comparison of the Central to Middle/Peripheral Groups

For a better overview, the groups, which are shown in Figure 12, were arranged into peripheral, middle and central groups. This arrangement is applied in Figure 13A and 13B to the mfVEP responses from DH and AY (as seen in Figures 8 and 9). There are three key findings illustrated in Figure 13A and 13B:

- For the central responses, the L- and M-cone modulations produce responses of similar amplitude and similar waveform for both subjects.
- For the middle and peripheral field, DH's responses are larger to L-cone modulation than to M-cone modulation, while AY's responses are approximately the same in amplitude.
- For the middle and especially for the peripheral field, DH's responses to L- and M-cone modulations differ in waveform, while AY's responses show similar waveform.

A. DH- 50%



B. AY-50%

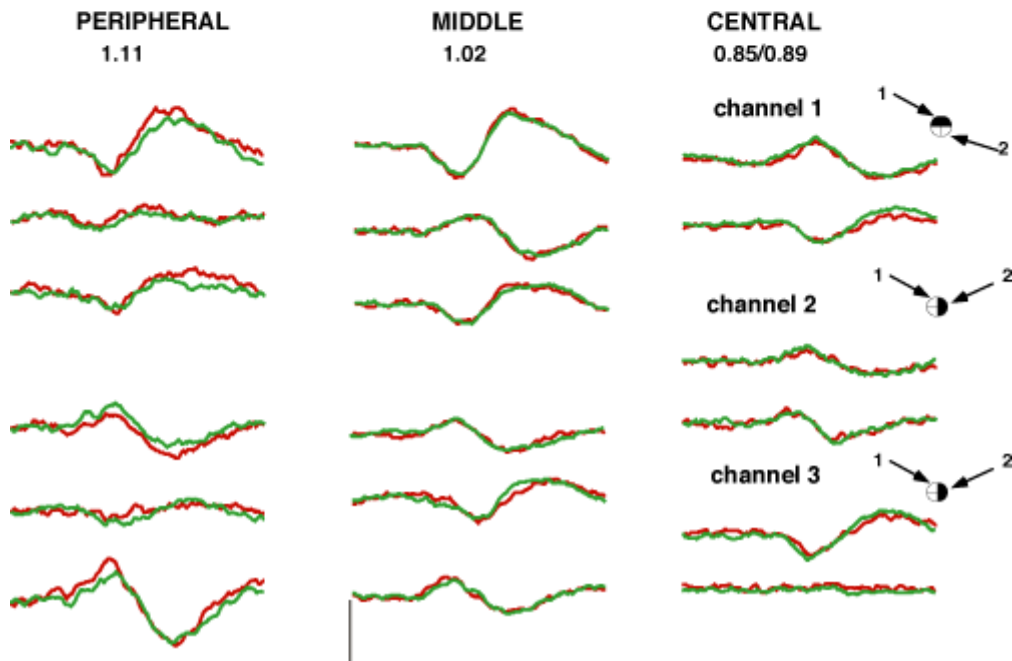


Figure 13. The summed mfVEP responses of subject DH and AY arranged into peripheral, middle and central groups. Channel 2 and 3 are added for the central groups. The numbers are the ratios of the root mean square (RMS) amplitudes to the L- versus the M-cone modulation. The calibration bars indicate 1 mV and 200 ms. (A) mfVEP responses to the 50% contrast condition for subject DH. (B) mfVEP responses to the 50% contrast condition for subject AY.

Figures 14 and 15 show this arrangement of groups in peripheral, middle and central groups for the other four subjects. For conciseness of presentation in Figure 14, responses for channel 2 and 3 are only shown for the half of the field with the larger responses. Following findings can be extracted from Figures 13, 14 and 15:

- For the central responses, the L- and M-cone modulations produce responses of similar amplitude and waveform for all six subjects (Figure 14).
- For the peripheral responses, the L- and M-cone modulations produce responses of different amplitude and waveform for most of the subjects (Figure 15), although there is a wide range of variation among individuals.
- The two extreme ends of the variation range is set by DH with the most apparent difference and AY with fairly similar amplitudes and waveforms for both cone modulations (Figure 13).

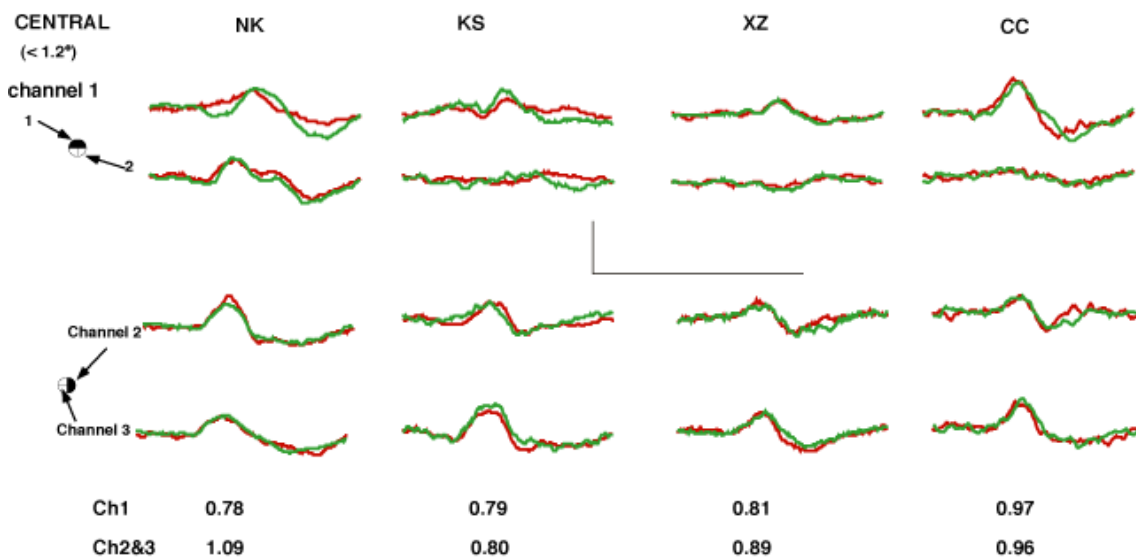


Figure 14. The summed mfVEP responses for the central groups from the four subjects NK, KS, XZ and CC. The numbers are the ratios of the root mean square (RMS) amplitudes to the L- versus M-cone modulation. The calibration bars indicate 1 mV and 200 ms.

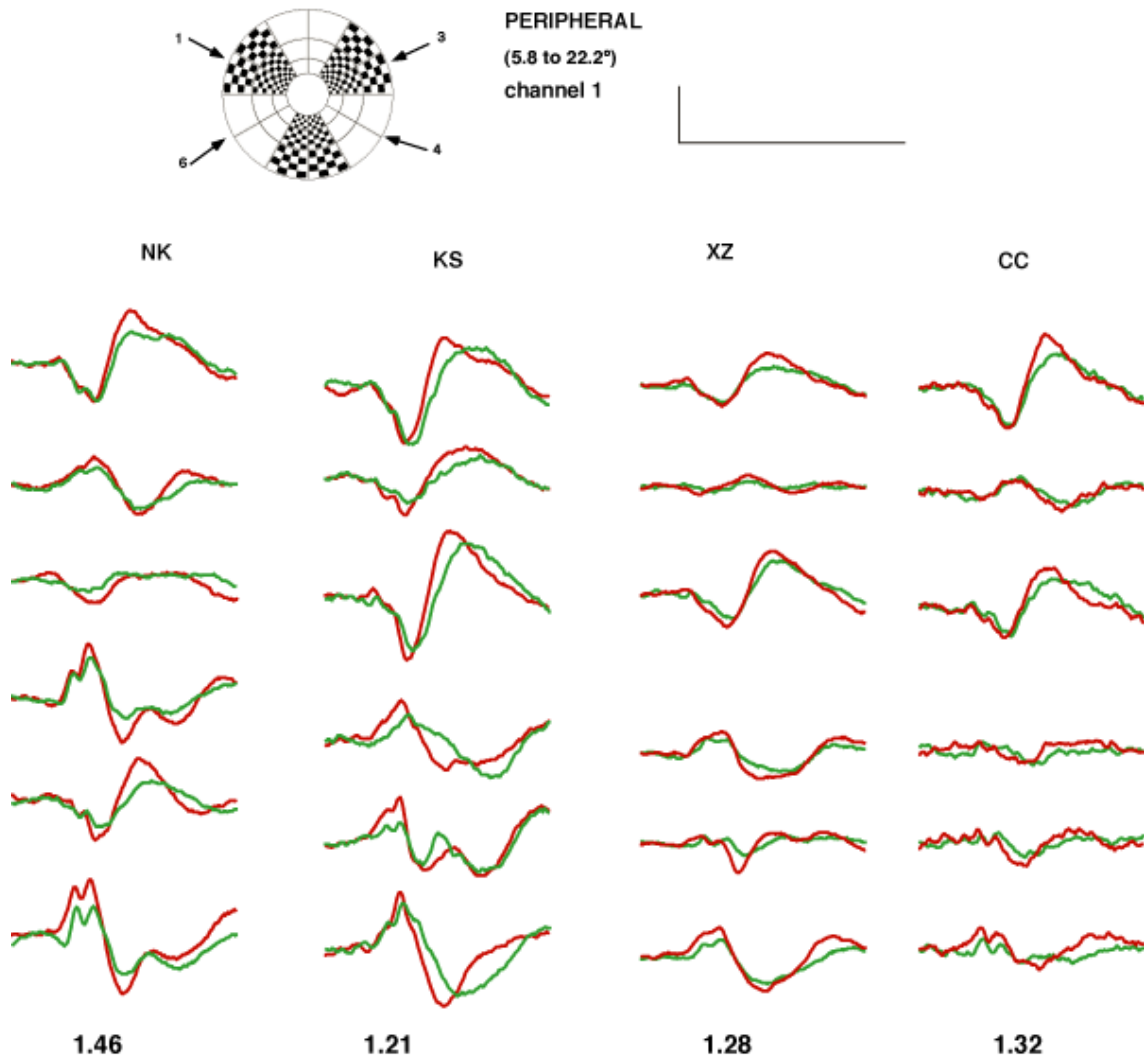


Figure 15. The summed mfVEP responses for the peripheral groups from the four subjects **NK**, **KS**, **XZ** and **CC**. The numbers are the ratios of the root mean square (RMS) amplitudes to the L- versus M-cone modulation. The calibration bars indicate 500 nV and 200 ms.

3.2.5 Root Mean Square (RMS) Ratio

The root mean square (RMS) is commonly taken to measure the response amplitude r_t at time t . It can be applied for all kinds of waveform and is calculated over some time interval, here 45 ms to 200ms, as

$$\text{RMS}_{\text{cone modulation}} = \left[\frac{\sum_{t=45}^{120} [r_t - u_{45to120}]^2}{N} \right]^{0.5}$$

where u_{45-120} is the average of the amplitudes from 45 to 120ms, and N is the number of samples in the time period. The relative amplitude of the responses to the L-cone and the M-cone modulations are represented in the relative ratio of their RMS amplitudes. The ratio of the RMS amplitudes for the L-cone and M-cone modulations is calculated as

$$\begin{aligned} & \text{ratio (L-cone-modulation / M-cone modulation)} \\ & = \text{RMS}_{\text{L-cone modulation}} / \text{RMS}_{\text{M-cone modulation}} \end{aligned}$$

The numbers above the responses in Figure 13 and below the responses in Figures 14 and 15 are the ratios of the summed RMS amplitudes for L- compared to the M-cone modulation. For example, the RMS amplitudes of DH's peripheral responses are 1.67 larger for the L-cone modulation than for the M-cone modulation.

For each of the peripheral records, the RMS amplitude was calculated and then summed, and the RMS ratios between the responses to the L- and M-cone modulations are shown in Figure 13 and 15. On average, for all six subjects, this summed RMS ratio is 1.34, with DH having the largest (1.67 for DH) and AY having the smallest (1.11 for AY) values.

For each of the central records, the RMS amplitude was calculated and then summed. The summed RMS ratios are shown in Figures 13 and 14 separately, one number for channel 1 and one for a combination of channel 2 and 3. On average, for all six subjects, these summed RMS ratios are 0.88 in the case of channel 1, and 0.95 in the cases of channel 2 and 3.

These results show that the RMS ratio for the central 1° is significantly lower than the ratio for the periphery both on average and for each of the six subjects. The ranges of the RMS ratios are nonoverlapping for each of the six subjects.

Table 9. RMS (L50/M50) for peripheral, middle and central responses

| RMS(L50/M50) | Peripheral | Middle | Central (ch1) | Central (ch2&3) |
|--------------|------------|--------|---------------|-----------------|
| DH | 1.67 | 1.70 | 1.08 | 1.09 |
| AY | 1.11 | 1.02 | 0.85 | 0.89 |
| NK | 1.46 | 1.40 | 0.78 | 1.09 |
| KS | 1.21 | 1.24 | 0.79 | 0.80 |
| XZ | 1.28 | 1.01 | 0.81 | 0.89 |
| CC | 1.32 | 1.26 | 0.97 | 0.96 |
| Mean Ratio | 1.34 | 1.27 | 0.88 | 0.95 |

3.2.6 Comparison of mfVEP Responses Summed in Six Rings

To exclude effects to our conclusions merely depending on our choice of groups, the RMS amplitudes were also obtained for each of the 60 individual responses and then summed for sectors of equal distance from the central fovea.

Table 10. RMS (L50/M50) for mfVEP responses summed in six rings

| RMS(L50/M50) | Ring 1 | Ring 2 | Ring 3 | Ring 4 | Ring 5 | Ring 6 |
|--------------|--------|--------|--------|--------|--------|--------|
| DH | 1.08 | 1.68 | 1.47 | 1.38 | 1.44 | 1.61 |
| AY | 0.84 | 0.97 | 1.13 | 1.08 | 1.10 | 1.15 |
| NK | 0.85 | 1.42 | 1.36 | 1.40 | 1.36 | 1.28 |
| KS | 0.93 | 1.19 | 1.08 | 1.24 | 1.21 | 1.41 |
| XZ | 0.93 | 0.98 | 1.09 | 1.18 | 1.27 | 1.33 |
| CC | 0.95 | 1.19 | 1.36 | 1.23 | 1.29 | 1.15 |
| Mean Ratio | 0.93 | 1.24 | 1.25 | 1.25 | 1.28 | 1.32 |

Figure 16 depicts the ratios of these summed RMS amplitudes versus the distance of the center of the sectors from the fovea. For example, the point at zero represents the ratio for the four central sectors, the next point for the eight sectors in the second ring and so on. It can be derived from Figure 16, that most of the differences in RMS ratio with eccentricity occur within 2° of the foveal center.

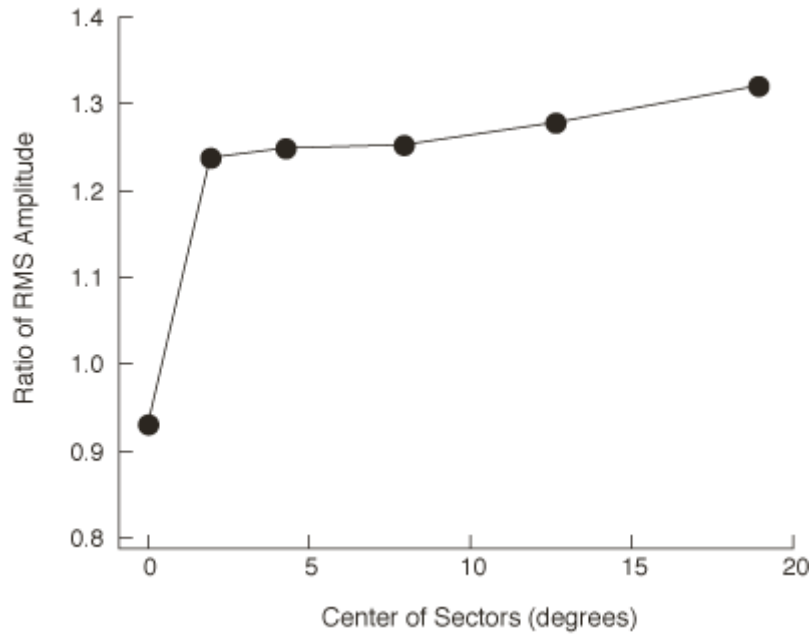


Figure 16. The mean (n=6) ratio of RMS amplitudes to the L- versus M-cone modulation as a function of the eccentricity of the center of the sectors.

3.2.7 Effects of Contrast

The responses in Figures 13, 14 and 15 were recorded for the 50% contrast condition. Figure 17 shows the results for the 25% contrast condition for the two subjects DH and AY with the most extreme ratios of RMS amplitudes to L- versus M-cone modulation. The mfVEP responses to the 25% contrast condition were grouped and summed as in Figure 12. Following findings can be extracted from Figure 17:

- For the central responses, the L- and M-cone modulations of 25% contrast produce responses of similar amplitude for both subjects.
- For the peripheral field, DH's responses to the L-cone modulation of 25% contrast tend to be larger than to the M-cone modulation, while AY's responses to the L- and M-cone modulation are similar in amplitude.
- Decreasing the contrast decreases the amplitude in all regions.
- In general, the results for the 25% contrast condition are the same as for the 50% contrast condition in Figure 13. Nonetheless, the waveform differences between DH's responses to L- versus M-cone modulation could not be overcome by a change in contrast.

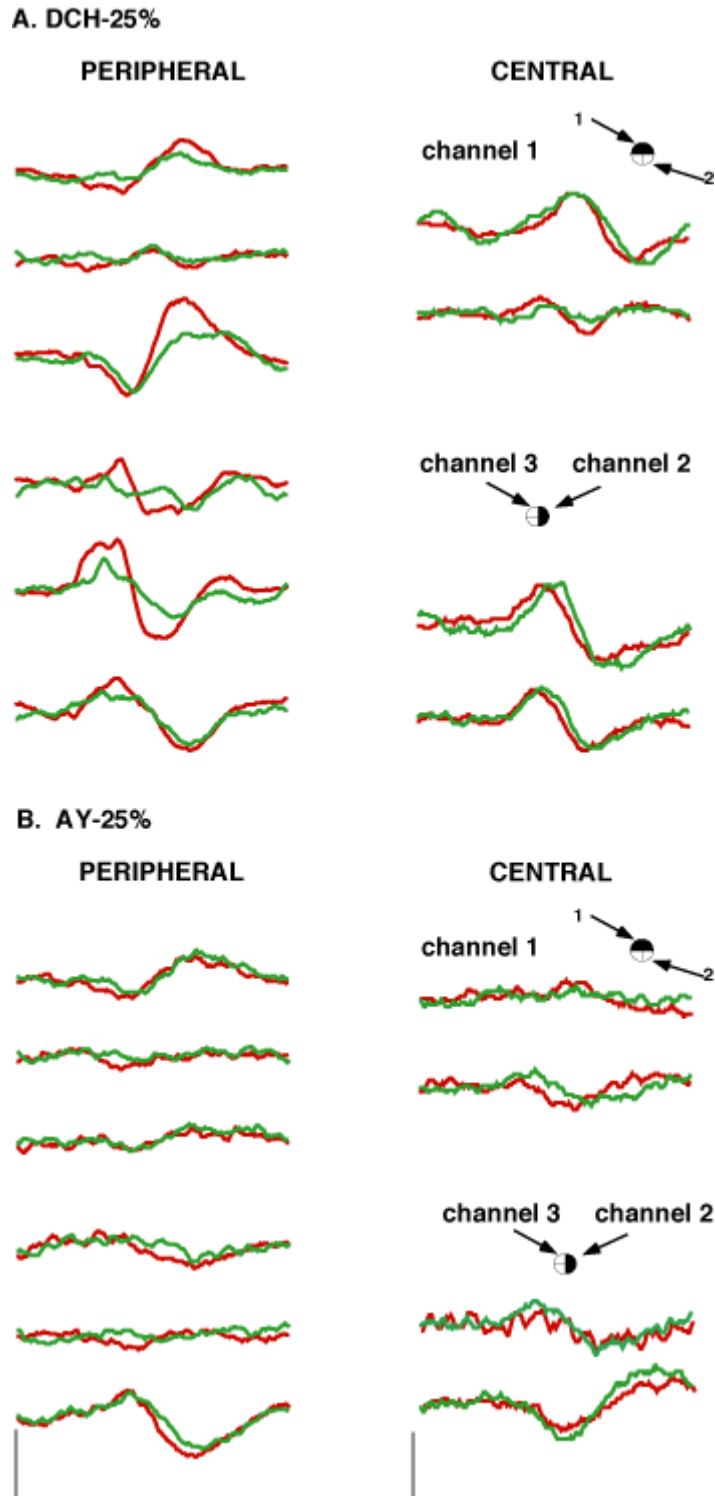


Figure 17. The summed mfVEP responses of subject DH and AY to 25% contrast condition. The vertical calibration bars indicate $1\mu\text{V}$ (left column) and 500 nV (right column) and the horizontal bars 200 ms . (A) The summed mfVEP responses to 25% contrast condition for the peripheral and central groups from subject DH. (B) The summed mfVEP responses to 25% contrast condition for the peripheral and central groups from subject AY.

Figure 18 shows a direct comparison between DH's responses to the 25% L-cone modulation and the 50% M-cone modulation. Following findings can be found in Figure 18:

- In the center, DH's responses to the 50% M-cone modulation are larger than those to the 25% L-cone modulation.
- In the periphery, DH's responses to the 25% L-cone modulation and the 50% M-cone modulation show more similar amplitudes than in the center. On average, the responses to the 25% L-cone modulation are slightly larger.
- For the peripheral responses, the responses to the left in Figure 18 were amplified by a factor of 3 and show that clear differences in waveform are still preserved between the L- and M-cone modulation in spite of bringing the amplitudes of the peripheral responses closer by reducing the contrast in the L-cone modulation. These differences can be seen in the relative amplitudes and implicit times of the local positive peaks, indicated with the dashed vertical lines, and are consistent within the most of DH's peripheral responses.
- For the central responses from channels 2 and 3, the responses of the L-cone modulation to the right in Figure 18 were amplified by a factor of 1.5 and show more similar waveforms as compared to the peripheral responses.

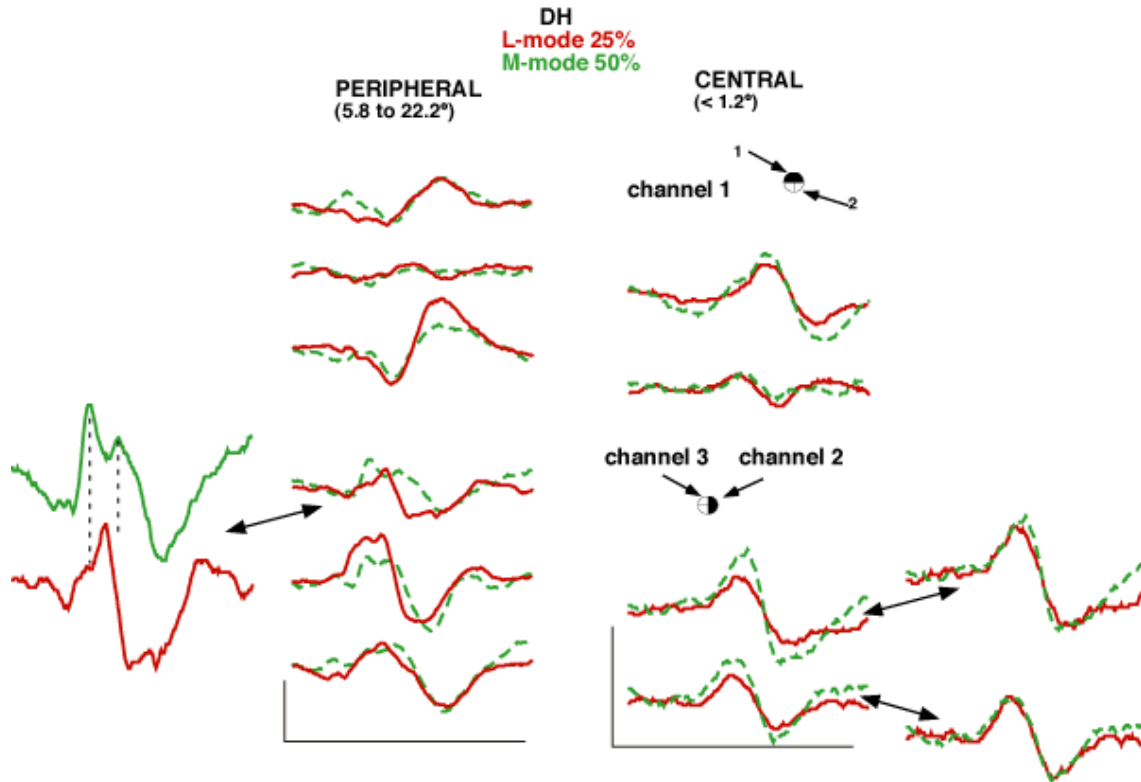


Figure 18. A comparison of DH's mfVEP responses elicited by the 25% L-cone modulation and the 50% M-cone modulation in the peripheral and central groups. The vertical calibration bars indicate 1 mV and the horizontal bars 200 ms.

For the six subjects, the RMS amplitudes for the L-cone modulation are 1.30 larger for the 50% contrast stimulus as compared to the 25% contrast stimulus. Similarly as described above, for the same six subjects, the ratio of the RMS amplitudes to L- versus M-cone modulation of 50% contrast is 1.34.

Table 11. RMS (L50/L25) for peripheral, middle and central responses

| RMS(L50/L25) | Peripheral | Middle | Central |
|--------------|------------|--------|---------|
| DH | 1.42 | 1.45 | 1.39 |
| AY | 1.46 | 1.40 | 2.04 |
| NK | 1.28 | 1.13 | 1.01 |
| KS | 1.16 | 0.98 | 0.55 |
| XZ | 1.27 | 1.00 | 0.74 |
| CC | 1.18 | 1.34 | 1.80 |
| Mean Ratio | 1.30 | 1.22 | 1.26 |

3.3 mfERG Studies

3.3.1 General Features of ERG Responses

It is known that a full-field flash ERG evokes a signal composing of a negative component, the a-wave, and a positive component, the b-wave. The a-wave is generated by photoreceptors, and thus the full-field flash ERG is a useful tool both for testing the scotopic rod functions in the peripheral retina and the photopic cone functions in the central retina. Under photopic conditions and high-frequency flicker stimulation, however, rods inputs are suppressed, and therefore only the cone functions are tested. The b-wave is generated in the middle retinal layer, including the bipolar cells, the horizontal cells, amacrine and müller cells.

On the other hand, the multifocal ERG signal consists of an initial negative deflection (N1), followed by a positive peak (P1), which are analogues of the a-wave and b-wave of the full-field flash ERG (Hood et al. 1997). In addition to that, there is also a second negative deflection (N2). Previous mfERG studies on monkeys showed that the N1 component is mainly produced by the OFF-bipolar cells, with relatively small contributions from the inner retina and the cone photoreceptors (Sieving et al. 1994; Horiguchi et al. 1998; Hood 2000; Hare et al. 2001; Hood et al. 2002a). The P1 component is largely generated by the onset of the ON-bipolar cells, and partly by the offset of the OFF-bipolar cells. The N2 component is predominantly elicited by the offset of both the ON-bipolar and OFF-bipolar cells (Hood et al. 2002).

3.3.2 Summed mfERG Responses to L- and M-cone Modulation

Figure 19 shows the mfERG records obtained in Tübingen, Germany from subjects DH and AY. To compare the L-cone to the M-cone modulation, which are depicted as red and green records, both records were overlaid on each other. Figure 19A and 19B depict the summed mfERG responses from the entire field, and Figure 19C the summed mfERG responses by annuli for DH. Following findings can be extracted from Figure 19:

- For DH, the peak-to-trough amplitude to the L-cone modulation is 225% larger than to the M-cone modulation (Figure 19A).
- For AY, the summed mfERG responses to L- and M-modulations are similar in amplitude. The peak-to-trough amplitude to the L-cone modulation is 10% smaller than to the M-cone modulation (Figure 19B).

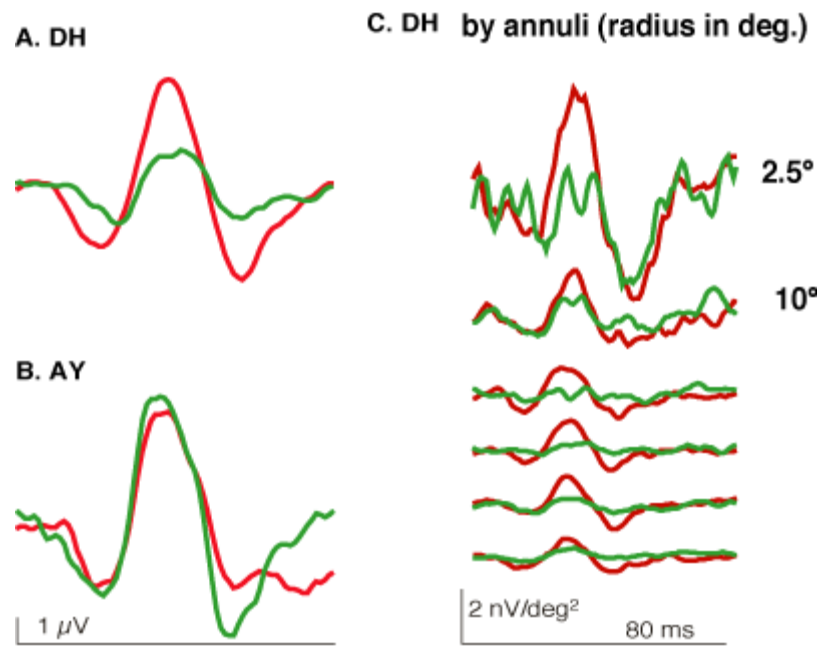


Figure 19. The summed mfERG responses of the subject DH and AY. (A) The mfERG responses summed over the the entire 103 hexagons for DH. (B) The mfERG responses summed over the the entire 103 hexagons for AY. (C) The mfERG responses summed by annuli for DH.

4 Discussion

4.1 Method Discussion

4.1.1 Reliability of the L- and M-cone-Isolating Stimuli

For the calibration of the monitor, the emission spectra of the phosphors of the monitor were only measured once at the maximum intensities of each phosphor, meaning at 100% red, 100% green and 100% blue phosphor. This had the advantage of reducing the systematic error, which could be caused by many measurements. It has to be noted that a spectroradiometer can be susceptible to interferences, especially to temperature fluctuations. Thus, plenty subsequent measurements during a longer time can be interfered by temperature changes (e.g. through repeated touch of the spectroradiometer), causing a systematic error.

In this study, the cone fundamentals of Stockman and Sharpe (1998; 1999; 2000), which were adjusted to trichromats and dichromats spectral sensitivities, were used. Those cone fundamentals were already chosen in previous studies by Kremers et al. (1999) and Kremers et al. (2000), who also calculated the L- and M-cone-isolating stimuli according to the silent substitution technique described by Estevez and Spekreijse (1982). In one of those studies (Kremers et al. 1999), the cone excitations by cone-isolating stimuli were recalculated by using another set of cone fundamentals, which resulted in only minor difference in the stimulus settings. Similarly, the recalculation, here in this study, with the cone fundamentals for 2° viewing conditions (Stockman and Sharpe 2000) in the reliability test showed only minor changes in the stimulus settings, insignificant for the evaluation of the mfVEP amplitudes.

To exclude any stimulation of cones other than the L-cones in the L-cone modulation and the M-cones in the M-cone modulation, the stimulus settings were adjusted to pre-studied calibration series obtained in Tübingen, Germany (see Albrecht et al. 2002). They yielded similar settings as the adjustment to the mfVEP data from a protanope and a deuteranope, when they showed no

residual cone response. These reliability tests were performed in order to confirm the precise silent substitution of the cone-isolating stimuli.

4.1.2 Difficulties in the mfVEP Recordings

The mfVEP recordings took place in an established setting in Donald C. Hood's laboratory, Psychology Department of Columbia University in New York, U.S.A., and were obtained in accordance with previous studies conducted in this laboratory [see (Hood et al. 2000a; Hood and Zhang 2000; Hood et al. 2000b)]. The major difference in this study was the display of cone-isolating stimuli instead of black-white dartboard arrays. The difficulty to generate responses from cone-isolating stimuli is largely due to the lower contrast between the red and green patches, in comparison to black versus white patches of the pattern-reversal dartboard. Therefore, in this study, cone contrast did not drop below 25%, since pre-study contrast series with e.g. only 12.5% cone contrast had shown to be too noise-overlapped. For this reason, the contrast settings were set at their maximal level to increase signal-to-noise ratio. Despite lifting the contrast to a maximum of 50% for the cone-isolating stimuli, their mfVEP responses were still smaller in amplitude than the responses to black-white pattern arrays. Given these conditions, it was of highest priority to reduce the noise to its lowest possible level in cone-isolating stimulus settings.

The most obvious prerequisite to reduce noise is a proper and clean electrode placement. The scalp-electrode impedances were checked before each recording, with the aim to achieve approximately 2 kOhms. High impedance was corrected by cleaning the scalp once again and replacing the electrodes. Furthermore, the positions of the scalp-electrodes are also of great importance. It has been shown that mfVEP recordings with multiple electrodes achieve higher signal-to-noise ratios (Hood et al. 2002b). Especially electrodes placed lateral to the midline seem to be beneficial for the central amplitudes (Klistorner and Graham 2000; Hood et al. 2002b). The disadvantages are mainly of practical nature: So does the placement of multiple electrodes require longer set-up time and higher costs, and also the data analysis and its

interpretation are more time-consuming and complex. Another source of noise is surrounding electronic instruments near the mfVEP equipments. Therefore all electronic instruments, which were not in use for the mfVEP recordings, were removed from the recording room. Lastly, the subject itself can generate a great amount of noise, for instance, by muscle artifacts or alpha-waves. However, this could be overcome by an awakened subject in a relaxing position.

The mfVEPs are known to be highly variable among individuals due to the variance in cortical anatomy and the orientation of the primary visual area in the cortex. However, the mfVEP data presents high reproducibility, when mfVEP responses of the same subject on different days are compared. This requires an accurate replacement of the electrodes according to an established arrangement of electrode positions as described in Figure 5. Against this background, the mfVEP has shown to be a useful clinical tool for detecting local damage to the optic nerve (Hood et al. 2000a; Hood and Zhang 2000; Hood et al. 2000b).

4.1.3 Difficulties in the mfERG Recordings

By the same line of arguments as for the mfVEP recordings, reducing noise and artifact are extremely important for mfERG recordings as well. In this study, the main source of noise during mfERG recordings came from the direct contact of the Nylon fibers of the DTL-electrodes to the subject's conjunctiva. Therefore anesthetic eye drops were offered to the subjects, who were sensitive to the Nylon fibers placed at the limb of the lower lid of their eye, in order to increase the subject's comfort and thus reduce blinking and muscle artifact.

4.1 Discussion of the Results

4.2.1 Foveal mfVEP and PC Pathway

The amplitudes and waveforms of the central responses to the L- and M-cone modulations appear to be similar for all six subjects, while they seem to differ in the peripheral responses.

It is known that there are two pathways, which receive major inputs from L- and M-cones, namely the MC and PC pathways. They can be tracked up to the human primary visual cortex surrounding the calcarine sulcus, the source of the mfVEPs, where stimuli are inverted and mapped on the contralateral hemisphere (Slotnick et al. 1999). Morphological studies with intracellular staining and recording have shown, that 95% of the total ganglion cells in the central retina between 2 and 6 mm eccentricity (equivalent to 0.34° and 1.01°) are midget ganglion cells projecting to the PC pathway (Dacey 1993). For this reason, it can be assumed that most mfVEP responses from the central 1.2° were recorded from the PC pathway. The similarity of the central mfVEP responses in waveform is also suggestive for the activation of a single pathway. Furthermore, midget ganglion cells were likely to be stimulated by the central segments of the mfVEP pattern, given their spectral opponency and their high sensitivities to chromatic contrast and high spatial frequency. At this point, the question arises why the central mfVEP responses produce similar amplitudes to L- and M-cone modulations.

There are two diverging hypotheses to this question, which are attributed to two different locations in the PC pathway. One hypothesis is based on a difference in the relative numbers of cones between the central and peripheral retina and particularly suggests an L/M cone ratio of approximately 1:1 in the retinal fovea (Krauskopf 2000). In contrary to that, the other hypothesis assumes a cone-type specific adjustment in the gain of the input to the PC pathway at or before the striate cortex, where the mfVEP is generated (Pokorny et al. 1991; Kremers et al. 2000; Otake and Cicerone 2000).

The hypothesis believing in an L/M cone ratio close to 1:1 in the central fovea is mainly defended by Krauskopf (2000). His flicker photometry studies with

foveal light of 2° diameter have shown that at high temporal frequencies (~30 Hz) the modulation sensitivity of L-cones is approximately twice of the modulation sensitivity of the M-cones, whereas low temporal frequencies (~2 Hz) trigger similar modulation sensitivities for both L- and M-cones. Krauskopf discussed two explanations: One interpretation assumed an L/M cone ratio of 2:1, given that the MC pathway gives equal weight to L- and M-cones and the PC pathway gives twice as much weight to the M-cones than to the L-cones. The other interpretation was based on an L/M cone ratio of 1:1, and that the MC pathway gives more weight to the L-cones than to the M-cones at higher temporal frequencies, while the PC pathway gives equal weight to both types of cones at low temporal frequencies. To further examine these contradictory interpretations, Krauskopf assembled and statistically analysed color appearance studies of small, brief, monochromatic lights, with the result that flashes are called red twice as often as green at approximately 600 nm. However, this was surprising given an L/M cone ratio of 2:1, since the observers were expected to locate the wavelength, at which they call twice as many flashes red as green, at approximately 570 nm, the wavelength where L- and M-cones are equally sensitive [according to the cone fundamentals of Smith and Pokorny (1975) and the field sensitivities of Stiles (1978)]. The comparison of the spectral sensitivities, as derived from these color-naming methods, with increment thresholds of the field sensitivities of L- and M-cones, measured on the same observers, showed close agreement. As the field sensitivities are assumed to be independent of the number of cone types, it was concluded that the L/M cone ratio is close to 1:1 in the central fovea and may not be so variable among individuals. However, it should be noted that this conclusion was derived from flicker photometry studies with a relatively larger fovea light of 2° diameter, whose low temporal frequencies were supposed to tap into the PC pathway. Thus, given that the midget ganglion cells are most highly concentrated in the central retina between 2 and 6 mm eccentricity, equivalent to 0.34° and 1.01° (Dacey 1993), it cannot be excluded that more than just the PC pathway was stimulated.

Until now, most estimates of L/M cone ratios for the central 2° or so come from behavioral data such as spectral sensitivity functions, HFPs or two-point detections. Their results diverge, though most researchers agree to an L/M cone ratio greater than 1.0 in the central fovea, but propose adjustment mechanisms in the central cone pathways. So did detection studies with small monochromatic lights imply stable, though inter-individual varying L/M cone ratios from fovea to midperiphery (± 28 deg nasotemporal) (Otake and Cicerone 2000). Consistent with the stability of the L/M cone ratio, the wavelength chosen as uniquely yellow remained unvarying over the same range of eccentricities, indicating a maintenance of red-green color appearance. However, findings saying that observers with different L/M cone ratios select similar wavelengths for unique yellow, appear to be suggestive for the existence of mechanisms in the cone pathways, which may achieve a standardization of color appearance. In another study, a combination of three different psychophysical tasks, namely detection thresholds for cone-isolating stimuli at different temporal frequencies, HFPs and cone contrast ratios at minimal flicker perception, as well as flicker ERG and retinal densitometry were applied in order to tap into the MC and PC pathways separately (Kremers et al. 2000). According to the sensitivity of the parasol ganglion cells, psychophysical tasks with high temporal frequencies as well as flicker ERGs and retinal densitometry yielded large inter-individual variations in L/M cone ratio. Opposed to that, psychophysical tasks with low temporal frequencies, similar to the sensitivity of midget ganglion cells, produced L/M cone ratios close to 1:1. These results imply a gain adjustment to compensate for the differences in L- and M-cone signal strength in the PC pathway, but not in the MC pathway, which may reflect the relative ratios of the cones. Lastly, a new approach as the direct visual imaging of the retina was combined with flicker ERG and the detection of unique yellow (Brainard et al. 2000). Again, the flicker ERG data yielded a stable variation in L/M cone ratio, whereas the small variation in the wavelength of unique yellow in the same two observers was assumed to be attributed to neural factors.

Convincing evidence is provided by Roorda and Williams (1999). Their technique achieved direct imaging of retinal patches within 1° of the foveal

center and confirmed large inter-individual variations in L/M cone ratio in the central retina. In addition to that, examinations of the L/M cone pigment mRNA in retinal patches of 23 human donor eyes elicited an L/M cone ratio of 1.5:1 in the central retina, which increased to 3:1 in the periphery of about 40° eccentricity (Hagstrom et al. 1998).

In face of these evidences, it is unlikely that the central 2° has a ratio close to 1:1 in all subjects. While DH's mfVEP responses from the central 1.2° are similar in amplitude, his mfERG responses from the central 2.5° are clearly larger for the L-cone modulation. These results indicate a gain adjustment in the PC pathway, after the mfERG is generated and before the mfVEP is elicited. As it is known that the mfERG, like the photopic full-field ERG, mainly represents bipolar responses (Sieving et al. 1994; Hood 2000; Hood et al. 2002a), it can be assumed that this gain adjustment occurs in the PC pathway after the bipolar cells respond, but before the cells in area 17 are activated, most likely in the inner plexiform layer before the ganglion cells are stimulated.

4.2.2 Peripheral mfVEP and MC Pathway

In the periphery, all subjects have different waveforms and larger amplitudes in their mfVEP responses to the L-cone modulation as compared to the M-cone modulation, except AY, whose responses to both cone modulations are similar in amplitude and waveform.

The peripheral mfVEP responses are considered as being some combined signals from the MC and PC pathways, evolving from receptive fields of the parasol and midget ganglion cells, which are large enough to receive the same L/M cone ratio of cones. Recordings with light-evoked voltage responses of H1 horizontal cells in the primate's retina showed that the L- and the M-cone inputs to the H1 horizontal cells reflect the L/M cone ratio in the H1 cell's receptive field (Dacey et al. 2000a). This leads to the assumption that this proportion may also be preserved in postreceptoral stages of the MC and PC pathways, which are the source of the mfVEP in the peripheral retina. To explain the qualitative differences in waveforms seen in most observers, the different features of MC and PC pathways need to be taken into consideration. The MC pathway is more

nonlinear and/or saturates at lower contrast than does the PC pathway. Therefore the cone contrast in this study is likely to evoke maximal responses in the MC pathway for both cone modulations, so that different L/M cone ratios achieve similar MC pathway activity. In contrary to that, the PC pathway is highly sensitive to chromatic contrast and saturates at a much higher contrast level. Thus, larger number of L-cones produces a larger PC pathway activity than do fewer M-cones, as the PC pathway has not reached its saturation level yet. Furthermore, according to the work of Baseler and Sutter (1997), MC and PC pathway show different waveforms in mfVEP recordings. Derived from these evidences, the responses to the L-cone modulation are larger due to a larger PC pathway contribution at high contrast. The waveforms to L-cone compared to M-cone modulation are different due to the different activities of MC and PC pathways in the periphery. The exception is seen in AY. AY's mfERG data implies an L/M cone ratio estimate of approximately 1:1. Thus, AY's responses are similar in amplitude and waveform, as the same number of L- and M-cones produces the same proportion of MC and PC pathway activities in the periphery.

4.2.3 Limitation of the mfVEP for L/M-cone Ratio Estimates

The mfVEP is not a particularly good way to estimate the variability in L/M cone ratio across the retina. The results of this study suggest that in the central fovea, a gain adjustment in the cone pathway has taken place before the mfVEP is generated. In the periphery, the mfVEP is considered as a combination of the MC and PC pathways. However, since at high contrast the MC pathway is already saturated to its maximal level independent of the cone numbers, a combined response from the MC and PC pathways is not linear to the numerosity of cones. Furthermore, the positive and negative portions of the MC and PC responses can both reinforce or cancel parts of the waveform. Other techniques for L/M cone ratio estimates are discussed below in 4.3.

4.2.4 Effects of Contrast Changes in the mfVEP

As in Figure 17, reducing the contrast to 25% in both cone modulations generates central responses of equal amplitude for DH and AY, and larger

peripheral responses for DH. This goes along with the above argument, that in the foveal center, the PC pathway activity dominates and undertakes a gain adjustment before the cells of area 17 are stimulated. As mentioned above as well, the peripheral responses are larger due to a larger PC contribution for the L-cone modulation. The MC pathway is thought to saturate around 10-15% contrast, and therefore still receive maximal saturation at a contrast of 25%. Reducing the contrast decreases the amplitude in all regions, as the height of the amplitudes in both the center and the periphery are mainly dependent on the PC pathway activity, given that the MC pathway in the periphery is already saturated at contrast levels above 10-15%.

As in Figure 18, the responses to 50% M-cone modulation are larger in the center compared to the responses to the 25% L-cone modulation for DH, since the central responses reflect the activity of the PC pathway, which is highly sensitive to chromatic contrast. However, both modulation show more similar amplitudes in the periphery with slightly larger responses to the 25% L-cone modulation. This observation is probably due to a balance between the effect of cone contrasts and cone inputs into the PC pathway. So is the 50% M-cone modulation assumed to elicit a high PC pathway activity due to higher chromatic contrast, but low PC pathway contribution due to the fewer M-cones in DH. Contrarily, the 25% L-cone modulation probably produces low PC pathway activity due to low contrast levels, but achieves high PC pathway contribution due to larger numbers of L-cones in the same subject. Decreasing contrast to bring the amplitudes of the peripheral responses closer, did not dissolve the difference in waveform for the L- and M-cone modulations. This is consistent with the assumption that the peripheral mfVEP responses are sums of MC and PC pathways, with their different contributions attributing to the different waveforms (Baseler and Sutter 1997). On the other hand, central mfVEP responses are likely to be generated by the sole PC pathway and thus have similar waveforms for both cone modulations.

Decreasing the contrast by half, the average RMS amplitude ratio for the 50% L-cone modulation to the 25% L-cone modulation is approximately 1.30, similar to the average RMS amplitude ratio of approximately 1.34 for the 50% L-

cone to the 50% M-cone modulation. Thus, the relative effectiveness of the L- and M-cone modulations is approximately equivalent to halving the contrast of the L-cone modulation. It is surprising that the average results are consistent with a linear summation of cone receptor signals, as it is typically assumed, and a L/M ratio of about 2. It is unclear if this is just a coincidence or if there are other mechanisms subserving cone contrast changes. Similarly to the H1 horizontal cells, it is worthwhile to ask if the L- and M-cone inputs are summed in proportion to the stimulus cone contrast in the MC and PC pathways as well (Dacey et al. 2000a). As for H1 horizontal cells, these L- and M-cone contrast gains are highly variable, since they are thought to reflect the mosaic of the L- and M-cones in their receptive fields.

4.2.5 Interpretation of the mfERG Results

The mfERG recordings were conducted in Lindsay T. Sharpe's laboratory, Division of Experimental Ophthalmology, University Eye Hospital, Tübingen, Germany, for DH and AY, the two subjects with the most extreme RMS amplitude ratios for the L- and M-cone modulations. For DH, the peak-to-trough amplitudes of the summed mfERG responses are 225% larger to the L-cone modulation than to the M-cone modulation. For AY, the mfERG responses are similar in amplitude.

In Albrecht et al. (2002), the L- and M-cone driven amplitude ratios of the summed inner 20° mfERG responses were compared with the L/M cone ratio estimates derived from HFP measurements for a 2° diameter. Especially the N1P1 component of the mfERG responses showed close correlation to the 2° HFP data for the same observers. This leads to the conclusion that the L/M cone ratios both in the central fovea and in the periphery vary among individuals, and that the L/M cone ratio for the central fovea highly correlates with the L/M cone ratio in the periphery within an individual. These results make it unlikely to believe in an abrupt L/M cone ratio change between the central fovea and the periphery. For DH, the mfERG responses in the central 2.5° show larger peak-to-trough-amplitudes for the L-cone than for the M-cone modulation,

suggesting larger L-cone than M-cone inputs to the central cone pathways at the bipolar level.

The mfERG is probably a less useful tool to examine the central responses, as the central mfERG responses are more noise-sensitive. Furthermore, there is evidence that a gain change of L- and M-cone signals may take place between the cone receptors and the bipolar cells depending on the eccentricity, since L- and M-cone driven mfERG amplitude ratios differ between central and peripheral retina (Albrecht et al. 2002).

4.3 Discussion of Various Techniques for L/M-cone Ratio Estimates

Since our understanding of postreceptoral color processing is still very vague, many different techniques have been developed and studied in order to estimate the variation in L/M-cone ratio across the retina and to learn more about the effect of the variation of cone ratios on postreceptoral pathways.

4.3.1 Heterochromatic Flicker Photometry (HFP)

The Heterochromatic Flicker Photometry (HFP) is a psychophysical method to obtain the spectral luminous efficiency function (LEF). The LEF, denoted $V(\lambda)$ function, describes the human spectral sensitivity to light within the visible spectrum under photopic daylight conditions. For the HFP, firstly a pre-procedural test is conducted, in which the subject determines the mean flicker threshold of a 2° reference light ($\sim 560\text{nm}$), which flickers with a frequency of $\sim 25\text{Hz}$. After that, the 2° reference light is presented in counterphase-alternation with a test light at high flicker frequency ($\sim 25\text{Hz}$). The subject then has to adjust the intensity of the flickering test light to a minimal subjective flicker perception. This procedure is repeated along nanometer wavelength-increments of the test light over the spectral range of 400 to 700 nm. Finally, the testing results can be depicted in an HFP function, which plots the overall spectral sensitivity of the subject, named as the LEF, against the tested wavelengths.

The LEF is only recruited by L- and M-cone spectral sensitivities, since appropriate filters in the background suppress the S-cones and high flicker rate (25Hz) saturates the rods. According to the CIE, L- and M-cone spectral sensitivities are described in cone fundamentals, which relate matching intensities of three cone primaries to the wavelength of monochromatic test light of equal energy. So did Smith and Pokorny (1975) fit cone primaries to the luminosity functions, determined by HFP procedures on protanopes and deuteranopes. It was De Vries (1946), who firstly suggested that the individual differences in the weighted sum of the L- and M-cone fundamentals could be mediated by the different proportions of L- and M-cones among individuals. His hypothesis was supported by Rushton and Baker (1964), who conducted HFP and retinal densitometry measurements on the same observers. Both methods yielded large inter-individual variations of L/M-cone ratios, but confirmed the same cone ratio for the same observer. In more recent approaches (Kremers et al. 2000), HFP functions were taken to provide an estimate of the L/M-cone ratio over the entire visible spectrum. HFP functions were fitted with weighted sum of the L- and the M-cone fundamentals of Stockman and Sharpe (1999; 2000), in which L/M-cone ratios were reflected by their relative weighting factors.

Although the HFP has become the most widely used method for estimating L/M-cone ratios, its application has been criticized by its accuracy and reliability. As light is firstly filtered by ocular media and inert macular pigments before transmitted to the photoreceptors, preretinal absorption may interfere with the measurements of the HFP. Other factors constraining the HFP accuracy include the different λ_{\max} of the photopigments' spectral sensitivities and the different optical densities of photopigments in each individual. To exclude these effects, the variable properties of photopigments were examined (Bieber et al. 1998). An algorithm-based model was used, where shifts in the λ_{\max} of photopigments were fitted to the L- and M-cone fundamentals of Smith and Pokorny (1975), and different optical densities of photopigments were simulated in order to generate LEFs. Deriving from this modelling experiment, it was concluded that both λ_{\max} shifts, especially variations in the L-cone sensitivity, and different

optical densities of photopigments can attribute to deviations in L/M-cone ratio estimates by HFPs. Another critical point for its accuracy is the logarithmic distortion of L/M-cone ratio estimates by HFPs (Carroll et al. 2000): Since the change in the relative quantity of cone numbers does not cause a proportional but a logarithmic change in spectral luminosity, a large change of cone ratio from e.g. 2:1 to 3:1 only produces a tiny change in the LEF by 0.05 log units, which is smaller than the usual error in HFP measurements.

4.3.2 Retinal Densitometry

The method of the retinal densitometry goes along with Rushton's principle of univariance: Regarding that each system only has one dimension of output, the intrinsic response of a photoreceptor to light is only determined by the effective quantal catch in the photopigment which produces pigment bleaching. Therefore photopigments do not recognize the wavelength property of light but only differ in their spectral sensitivities of quantal absorption. Based on this principle, Rushton and Baker (1964) were the first using the retinal densitometry according to the following procedure: A measuring light consisting of two beams, one beam of deep red (700 nm) unabsorbed by any visual pigment and serving as a control and another beam with 610 or 535 nm, is sent into the dilated eye through a 2° centered aperture. The light's quantal energy is partially absorbed by the photopigments, whereas the non-absorbed part of the light's energy is reflected from the fundus oculi. A photometric wedge in the 700 nm beam sets both beams to the same luminance. The measuring light is rapidly alternated to a bleaching light at about 10 times per second in order to obtain equilibrium conditions of bleaching. Gradual increase of the bleaching lights causes changes in the luminance registered by the photometric wedge, which reflects the change in density of the cone pigments.

Kremers et al. (2000) applied the method of retinal densitometry of Rushton and Baker to generate four different reflectance measurements: They measured the reflection spectra for the red and green photopigments both in light- and dark-adapted conditions. The four reflection spectra obtained in each subject were then analysed with a model for fundus reflectance, which considered the

absorption and reflection of different retinal layers as well as of the spectral extinction spectra (van de Kraats et al. 1996). A simultaneous fitting of the four measured spectra yielded an estimate of the optical pigment densities and thus an estimate of the L/M-cone ratios.

4.3.3 Flicker-Photometric ERG

Another method to measure the spectral luminosity function is the flicker-photometric electroretinogram (ERG), which is recorded by a three-channel Maxwellian-view optical system consisting of one test beam, one reference beam and one adaptation beam. A monochromatic test light is created by an electronically tunable computer-controlled liquid-crystal filter. It interferes with an achromatic reference light from a second beam. The test light and the reference light are rapidly alternated ($\sim 30\text{Hz}$) with interposed off period phases. A circular neutral-density wedge helps to adjust the intensity of the test light to a value, until it produces an ERG amplitude comparable to that produced by the reference light. Thus, during the overall test session a null response of the ERG monitors equal intensity levels of the test and the reference lights. The spectral luminosity function of the tested individuals can be measured by increasing the wavelength of the test light at nanometer increments over a range of up to 400-700 nm.

To exclude the error of variable λ_{max} , Carroll et al. (2000) extracted photopigment gene sequences from each subject's DNA samples in order to obtain the individual λ_{max} . The individual λ_{max} could then be matched to individual L- or M-cone fundamentals by using a wavelength-shiftable visual pigment template curve. Lastly, the L/M-cone ratios were estimated by finding the weighted sum of L- and M-cone fundamentals required for the best fit of the spectral sensitivity data. In contrary to the HFP, the flicker-photometric ERG is regarded of being more objective, as the intensity of the test light depends on the electrophysiological ERG amplitude. Additionally, it is also viewed as a more accurate method: While variations in the macular pigment is mostly concerned for recordings in the fovea, the stimulus of the flicker-photometric ERG illuminates a vast retinal area, subtended up to 70° . Thus, the ERG signal is

mainly created by peripheral cones with short cone outer segments, which ensures a more consistent optical density of photopigments.

4.3.4 mRNA Analysis

There is a rich variety of the number and arrangement of cone pigment genes on the X- chromosome including spectrally distinct subtypes of L and M pigment genes, which allows expression of more than three spectrally distinct cone pigment genes. To assess which genes are expressed, Hagstrom et al. (2000) examined photopigment messenger RNAs (mRNAs) from retinal homogenates derived from human donor eyes. They collected single cones from midperipheral retinal regions in approximately 10° to 20° eccentricities. The mRNA was then amplified by polymerase chain reaction (PCR), cleaved with restriction endonuclease and finally visualized by either a phosphor imaging or fluorescence method. For midperipheral patches of retina, their results suggested that the relative L/M mRNA levels are consistent with the counting of single L and M cells in the same cadaver eyes, although inter-individual variation exists. Previous studies of the relative amount of L- to M-cone opsin gene expression were conducted on 23 human donor eyes for different retinal locations (Hagstrom et al. 1998). For the central retina, the average L/M mRNA ratio was about 1.5:1 and increased to 3:1 for the far periphery of approximately 40° eccentricity. The L/M mRNA ratios differed largely among individuals up to a factor of more than 3 for central retinal patches. This method for quantification of differences in mRNA has its limitations in errors during the isolation and sequence analysis of the mRNA. Contaminations by mRNA of lysed cells or incomplete enzyme digestions are examples of such errors.

4.3.5 Direct High-Resolution Imaging of the Retina

Direct imaging of the living human retina provided the first images of the arrangement of L-, M- and S-cones. This progressive method of combining direct retinal imaging with retinal densitometry was firstly applied by Roorda and Williams (1999). They developed a scanning laser ophthalmoscope with

adaptive optics, a system of segmented mirrors similar to those used in ground-based telescopes, which helps to refocus stray photons to a point and thus improves the lens's resolution by fourfold, enough to image single retinal cells. Repeated pictures of the same small patch of retina (about 30-40 arc min in diameter) were taken in a dark-adapted state. Afterwards, they were compared to fully bleached images in order to detect S-cones, then compared to images taken after a 650 nm light had selectively bleached the L pigments, and to images taken after a 470 nm light had selectively bleached the M pigments. Finally absorption images from those images showed the distribution of the classified cones and allowed estimates of the L/M-cone ratio. These measurements were conducted on two retinal patches for each of two male subjects with normal color vision, one at a retinal eccentricity of one degree nasal and one at a retinal eccentricity of one degree temporal of the foveal centre. Their results directly confirmed large individual differences in the L-/M-cone ratio in the central retina. Convincing as this results have been, direct retinal imaging is still regarded as a very demanding technique at the forefront of its development. Not until the size and the costs for the apparatus are reduced, it will remain hard to establish its broad use as a representative counts from humans.

4.3.6 Microspectrophotometry of Single Cones

The microspectrophotometry is a method to obtain the absorbance spectra of the outer segment of cones. For this purpose, a measuring beam transversely passes through isolated outer segments of cones and thus yields the mean absorbance spectra of all three cones with their different λ_{\max} , which appear to reflect the spectral sensitivities of the cones (Bowmaker and Dartnall 1980; Dartnall et al. 1983).

4.3.7 Monochromatic Light Detection

The probability of detecting a point-source stimulus of a particular intensity is highly dependent on the sample of cones that it affects. Detection occurs when any of the illuminated cones absorbs the required number of quanta. Cicerone

and Nerger (1989) presented small, brief, monochromatic test lights of 1 min visual angle in the fovea centralis. Yes-no detection reports were gathered for the spectral range between 520 nm and 660 nm. To the observers, the color of the tiny test lights appeared to be either red or green varying from individual to individual. This was attributed to the relative number of effective cone type activation. As the stimulus was so small, only few cones were illuminated. Thus, the number of the activated cone type affected the probability of the detection function. Detection functions were measured on six color normal observers and yielded L/M-cone ratio estimates ranging between 1.46:1 and 2.36:1. Similarly, Otake and Cicerone (2000) used a standard three-channel Maxwellian-view apparatus to study the relative number of L- to M-cones from the fovea to the midperipheral retina. One channel presented a monochromatic test light stepwise along the horizontal meridian from the fovea up to the 28° eccentricity for both the nasal and temporal retina. The stimulus sizes were chosen so that they illuminated the same amount of cones at each eccentricity. The two other channels were responsible for the 7° background field. Rods were bleached by a white light and by carefully selected adapting background fields, to allow L- and M-cones being tested separately: The monochromatic test light was set at 640 nm on a 500 nm background field to favor L-cone detection, and at 520 nm on a background field, composed of a mixture of 460 nm and 640 nm lights, to favor M-cone detection. The intensity of the test light was then logarithmically increased for each eccentricity. The observer was asked to determine the degree of certainty that the test light was seen. The psychometric function of detection yielded the relative numerosity of the L- and M-cones, which were stable from the fovea to the midperipheral retina for each observer.

4.3.8 Detection of Unique Yellow

Otake and Cicerone (2000) applied the same study design like in the monochromatic light detection experiment on the same observers, however, this time they changed the test light to unique yellow. Unique yellow is considered as the wavelength, which is created by a balanced contributions of the L- and M-cones to the opponent red-green channel. A force-choice experiment

determined the wavelength of the unique yellow, by adjusting the intensity of the test light until the observers declared it being neither reddish nor greenish. These results showed that the unique yellow wavelengths were invariant from fovea to midperiphery ($\pm 28^\circ$ nasotemporal) and were consistent with the stability in red-green color appearance and the stability in the relative number of the L- to M-cones over this range of eccentricities.

4.3.9 Foveal Cone Detection Thresholds

Extensive studies on the foveal cone detection threshold were conducted by Wesner et al. (1991). One or two brief (0.5 ms) point sources of light with a visual angle of 1 min were simultaneously presented at randomly different foveal locations. As the two points were only separated by 17 mins, the observers were asked to report seeing either 0, 1 or 2 flashes of lights. By incrementally increasing the radiance level, the one-to-two flash detections conjured up a psychometric function, usable to estimate the foveal L/M-cone proportions.

4.3.10 Red-Green Equiluminance Points

As described above, the luminous efficiency function constitutes the weighted sum of the L- and M-cone fundamentals, referring to a weighted sum of L- and M-cone excitations. It can be derived from this model of human spectral sensitivity that two lights at equiluminance must have the same weighted sum of L- and M-cone excitations. In a study of Dobkins et al. (2000), the subjects were asked to adjust the red-green luminance contrast of a moving heterochromatic grating to minimal moving perception, which yielded the red-green equiluminance points. The L- and M-cone excitations were then depicted as spectral functions of the red and green peaks of the gratings at the average equiluminance point. By cross-multiplication of the spectral functions with the L- and M-cone fundamentals of Stockman et al. (1993), an estimate of the relative numerosity of L- and M-cones could be calculated.

4.3.11 Flicker Detection Thresholds and Minimal Flicker Perception

There is evidence that flicker sensitivities to L- and M-cone modulations vary with changes in the temporal frequencies of the stimuli. In a study of Kremers et al. (2000), sinusoidally modulated L- or M-cone-isolating stimuli with a stimulus field of 4° diameter were presented at different temporal frequencies. The cone contrasts were modulated in order to determine the flicker detection thresholds for different temporal frequencies. Finally, the L- and M-cone contrast sensitivities could be used to calculate the proportions of L- to M-cones. In another experiment of the same study, the subjects were asked to adjust the cone contrast ratio for sine-wave stimuli to a minimal flicker perception. Direct estimates of L/M-cone ratios were then derived from the change of the modulation depths of the red and green phosphors. Both experiments resulted in a greater L- to M-cone proportion for high temporal frequency testing, whereas testing conducted at low temporal frequencies revealed similar L- and M-cone proportions. Similarly, in a study of Krauskopf (2000), the temporal modulation sensitivities of L- and M-cones were measured with an odd-symmetric temporal Gabor stimuli spanning a circle area of 2° diameter, which varied the inputs of either only the L- or only the M-cones. Their results showed that the modulation sensitivity of L-cones was approximately twice that of M-cones at higher temporal frequencies, but similar at lower frequencies. Thus, they concluded that equal numbers of L- and M-cones may exist, and that it may have been the MC and PC pathways, which assigned different weights to both types of cone at different temporal frequency levels.

4.4 Conclusion

The variation in the relative RMS amplitude ratio and the waveform of mfVEP responses to L- and M-cone modulations are likely to be due to the differences in the ratio of the L/M cone input to both the MC and PC pathways. The similarities in amplitude and waveform of the central responses for all subjects can be attributed to an L/M cone ratio close to 1.0 in the central 1° and/or a gain adjustment of the L- versus M-cone contributions to the central PC pathway. Evidence from other techniques, as well as the mfERG results from Albrecht et al. (2002), suggest the latter. The central mfVEP responses mainly tap into the PC pathway, which is also reflected in the similarity of their waveforms. For one observer, mfERG records from the central 2.5° were obtained, which show clearly larger responses to the L-cone than to the M-cone modulation, whilst the mfVEP responses from the central 1.2° from the same observer remain similar in amplitude. These results support a gain adjustment of the L- versus the M-cone contributions in the central PC pathway after the bipolar cells respond, but before the cells in area 17 are activated, most likely in the inner plexiform layer. This gain adjustment in the central PC pathway may be considered for optimizing foveal hue discrimination in the red-green region of the spectrum among observers.

The mfVEP is not a particularly good way to estimate the variation in L/M cone ratio across the retina, while other techniques still leave room for improvement. To sum up, the mfVEP is useful to examine the implications of L/M cone ratio in the PC and MC pathways by bridging between the physiology and anatomy of primates including humans and behavioural data from the humans.

5 Summary

We conducted mfVEP recordings to L- and M-cone-isolating stimuli on six color-normal trichromats. The relative RMS amplitudes of the mfVEP responses to the L- and M-cone modulations of equal cone contrast seemed to differ between the central fovea and the periphery. In the central 1.2° of visual field, the RMS amplitude ratios of the mfVEP responses to the L- and M-cone modulations showed only small variations between 0.8 and 1.1 among individuals, with an average ratio of approximately 0.9. On the other hand, in the more peripheral responses outside the central 5.8° radius, the RMS amplitude ratios varied between 1.1 and 1.7, with an average ratio of approximately 1.34. Furthermore, there were differences in waveform of the mfVEP responses in the fovea compared to those in the periphery as well. The central responses to the L- and M-cone modulations were similar in waveform for all subjects. In contrary, the waveforms of the peripheral responses to L- and M-cone modulations differed for most subjects. The clear exception was AY, the subject, whose mfERG records suggested an approximately equal number of L- and M-cones. Her mfVEP responses to L- and M-cone modulations were similar in waveform for both the central fovea and the periphery.

Reducing the contrast for both the L- and M-cone modulation did not seem to bring the waveforms for both cone modulations closer. Interestingly, the RMS amplitude for the 50% L-cone modulation was 1.30 larger than for the 25% L-cone modulation, similar to the average RMS amplitude ratio of approximately 1.34 for the 50% L-cone to the 50% M-cone modulation. Thus, the relative effectiveness of the L- and M-cone modulations is approximately equivalent to halving the contrast of the L-cone modulation.

The substantially lower ratio for the central responses is consistent with an L/M cone ratio close to 1.0 in the central 1° and/or a gain adjustment of the L-versus M-cone contributions to the central PC pathways. Evidence from other techniques, as well as the mfERG results from two observers support the latter. It appears that a gain adjustment of the L- versus the M-cone contribution in the

central PC pathway takes place after the bipolar cells respond, but before the cells in area 17 are activated, most likely in the inner plexiform layer.

6 Appendix

6.1 Screen Calibration Table

| | | Phosphor's energy in | | | |
|-------------|--------|----------------------|--------|-------------|--------|
| Veris scale | % | Veris scale | % | Veris scale | % |
| 1 | 0.0006 | 35 | 0.0960 | 69 | 0.4364 |
| 2 | 0.0007 | 36 | 0.1022 | 70 | 0.4506 |
| 3 | 0.0009 | 37 | 0.1087 | 71 | 0.4651 |
| 4 | 0.0013 | 38 | 0.1153 | 72 | 0.4799 |
| 5 | 0.0018 | 39 | 0.1222 | 73 | 0.4949 |
| 6 | 0.0024 | 40 | 0.1293 | 74 | 0.5102 |
| 7 | 0.0031 | 41 | 0.1366 | 75 | 0.5257 |
| 8 | 0.0041 | 42 | 0.1441 | 76 | 0.5415 |
| 9 | 0.0051 | 43 | 0.1519 | 77 | 0.5576 |
| 10 | 0.0063 | 44 | 0.1598 | 78 | 0.5739 |
| 11 | 0.0077 | 45 | 0.1681 | 79 | 0.5905 |
| 12 | 0.0092 | 46 | 0.1765 | 80 | 0.6073 |
| 13 | 0.0110 | 47 | 0.1852 | 81 | 0.6244 |
| 14 | 0.0128 | 48 | 0.1941 | 82 | 0.6417 |
| 15 | 0.0149 | 49 | 0.2032 | 83 | 0.6594 |
| 16 | 0.0171 | 50 | 0.2126 | 84 | 0.6773 |
| 17 | 0.0195 | 51 | 0.2222 | 85 | 0.6954 |
| 18 | 0.0221 | 52 | 0.2320 | 86 | 0.7138 |
| 19 | 0.0249 | 53 | 0.2421 | 87 | 0.7325 |
| 20 | 0.0278 | 54 | 0.2524 | 88 | 0.7515 |
| 21 | 0.0310 | 55 | 0.263 | 89 | 0.7707 |
| 22 | 0.0343 | 56 | 0.2738 | 90 | 0.7902 |
| 23 | 0.0379 | 57 | 0.2848 | 91 | 0.8099 |
| 24 | 0.0416 | 58 | 0.2961 | 92 | 0.8300 |
| 25 | 0.0455 | 59 | 0.3076 | 93 | 0.8503 |
| 26 | 0.0496 | 60 | 0.3194 | 94 | 0.8708 |
| 27 | 0.0540 | 61 | 0.3314 | 95 | 0.8917 |
| 28 | 0.0585 | 62 | 0.3436 | 96 | 0.9128 |
| 29 | 0.0632 | 63 | 0.3561 | 97 | 0.9342 |
| 30 | 0.0682 | 64 | 0.3689 | 98 | 0.9559 |
| 31 | 0.0733 | 65 | 0.3819 | 99 | 0.9778 |
| 32 | 0.0787 | 66 | 0.3951 | 100 | 1.0000 |
| 33 | 0.0842 | 67 | 0.4086 | | |
| 34 | 0.0900 | 68 | 0.4224 | | |

6.2 Index of Figures

| | |
|--|----|
| 1. Emission spectra of the three phosphors as measured by the spectroradiometer. | 18 |
| 2. Quanta spectrum of the three phosphors. | 19 |
| 3. Cone fundamentals for 10°. | 19 |
| 4. The stimulus array for the mfVEP recordings. | 35 |
| 5. Electrode positions and configurations for the three channels of recording. | 36 |
| 6. The stimulus array for the mfERG recordings. | 39 |
| 7. A single VEP signal to pattern-reversal. | 44 |
| 8. The 60 mfVEP responses of subject AY to the L-cone (red traces) and M-cone (green traces) modulations at 50% contrast condition from channel 1. | 45 |
| 9. mfVEP responses to 50% contrast condition from channel 1 for subject DH. | 46 |
| 10. mfVEP responses to 50% contrast condition from channel 2 for subject DH. | 46 |
| 11. mfVEP responses to 50% contrast condition from channel 3 for subject DH. | 47 |
| 12. Grouping of the mfVEP responses. | 48 |
| 13. The summed mfVEP responses of subject DH and AY arranged into peripheral, middle and central groups. | 50 |
| 14. The summed mfVEP responses for the central groups from the four subjects NK, KS, XZ and CC. | 51 |
| 15. The summed mfVEP responses for the peripheral groups from the four subjects NK, KS, XZ and CC. | 52 |
| 16. The mean (n=6) ratio of RMS amplitudes to the L- versus M-cone modulation as a function of the eccentricity of the center of the sectors. | 55 |
| 17. The summed mfVEP responses of subject DH and AY to 25% contrast condition. | 56 |
| 18. A comparison of DH's mfVEP responses elicited by the 25% L-cone modulation and the 50% M-cone modulation in the peripheral and central groups. | 58 |
| 19. The summed mfERG responses of the subject DH and AY. | 60 |

6.3 Index of Tables

| | |
|--|----|
| 1. Subject information | 16 |
| 2. Veris scale for the calculated L-cone modulation | 24 |
| 3. Veris scale for the L50 setting | 27 |
| 4. Veris scale for the L25 setting | 27 |
| 5. Veris scale for the calculated M-cone modulation | 28 |
| 6. Veris scale for the M50 setting | 31 |
| 7. Veris scale for the M25 setting | 31 |
| 8. Stimulator parameters in the Veris 4.2 setting | 33 |
| 9. RMS (L50/M50) for peripheral, middle and central responses | 54 |
| 10. RMS (L50/M50) for mfVEP responses summed in six rings | 54 |
| 11. RMS (L50/L25) for peripheral, middle and central responses | 58 |

7 References

- Ahnelt, P. K., Kolb, H., Pflug, R. (1987)
Identification of a subtype of cone photoreceptor, likely to be blue sensitive, in the human retina.
Journal of Comparative Neurology **255**: 18-34.
- Ahnelt, P., Keri, C., Kolb, H. (1990)
Identification of pedicles of putative blue-sensitive cones in the human retina.
Journal of Comparative Neurology **293**: 39-53.
- Albrecht, J., Jägle, H., Hood, D. C., Sharpe, L. T. (2002)
The multifocal electroretinogram (mfERG) and cone isolating stimuli: Variation in L- and M-cone driven signals across the retina.
Journal of Vision **2**(2): 543-558.
- Baseler, H. A., Sutter, E. E., Klein, S. A., Carney, T. (1994)
The topography of visual evoked response properties across the visual field.
Electroencephalography and Clinical Neurophysiology **90**(1): 65-81.
- Baseler, H. A., Sutter, E. E. (1997)
M and P components of the VEP and their visual field distribution.
Vision Research **37**(6): 675-690.
- Benardete, E. A., Kaplan, E., Knight, B. W. (1992)
Contrast gain control in the primate retina: P cells are not X-like, some M cells are.
Visual Neuroscience **8**: 483-486.
- Bieber, M. L., Kraft, J. M., Werner, J. S. (1998)
Effects of known variations in photopigments on L/M cone ratios estimated from luminous efficiency functions.
Vision Research **38**(13): 1961-1966.
- Bowmaker, J. K., Dartnall, H. J. (1980)
Visual pigments of rods and cones in a human retina.
Journal of Physiology **298**: 501-511.
- Brainard, D. H., Roorda, A., Yamauchi, Y., Calderone, J. B., Metha, A., Neitz, M., Neitz, J., Williams, D. R., Jacobs, G.H. (2000)
Functional consequences of the relative numbers of L and M cones.
Journal of the Optical Society of America. A, Optics, Image Science, and Vision **17**(3): 607-614.

- Calkins, D. J., Schein, S. J., Tsukamoto, Y., Sterling, P. (1994)
M and L cones in macaque fovea connect to midget ganglion cells by different numbers of excitatory synapses.
Nature **371**(6492): 70-72.
- Calkins, D. J., Tsukamoto, Y., Sterling, P. (1998)
Microcircuitry and mosaic of a blue-yellow ganglion cell in the primate retina.
Journal of Neuroscience **18**: 3373-3385.
- Carroll, J., McMahon, C., Neitz, M., Neitz, J. (2000)
Flicker-photometric electroretinogram estimates of L:M cone photoreceptor ratio in men with photopigment spectra derived from genetics.
Journal of the Optical Society of America. A, Optics, Image Science, and Vision **17**(3): 499-509.
- Cicerone, C. M., Nerger, J. L. (1989)
The relative numbers of long-wavelength-sensitive to middle-wavelength-sensitive cones in the human fovea centralis.
Vision Research **29**(1): 115-128.
- Curcio, C. A., Sloan, K. R., Packer, O., Hendrickson, A. E., Kalina, R. E. (1987).
Distribution of cones in human and monkey retina: individual variability and radial asymmetry.
Science **236**: 579-582.
- Curcio, C. A., Allen, K. A., Sloan, K. R., Lerea, C. L., Hurley, J. B., Klock, I. B., Milam, A. H. (1991)
Distribution and morphology of human cone photoreceptors stained with anti-blue opsin.
Journal of Comparative Neurology **312**: 610-624.
- Dacey, D. M., Petersen, M. R. (1992)
Dendritic field size and morphology of midget and parasol ganglion cells of the human retina.
Proceedings of the National Academy of Sciences of the United States of America **89**(20): 9666-9670.
- Dacey, D. M. (1993)
The mosaic of midget ganglion cells in the human retina.
Journal of Neuroscience **13**(12): 5334-5355.
- Dacey, D. M., Lee, B. B. (1994)
The blue-ON opponent pathway in primate retina originates from a distinct bistratified ganglion cell type.
Nature **367**: 731-735.

- Dacey, D. M. (1999)
Primate retina: cell types, circuits and color opponency.
Progress in Retinal Research **18**(6): 737-763.
- Dacey, D. M., Diller, L. C., Verweij, J., Williams, D. R. (2000a)
Physiology of L- and M-cone inputs to H1 horizontal cells in the primate retina.
Journal of the Optical Society of America. A, Optics, Image Science, and Vision **17**(3): 589-596.
- Dacey, D. M., Packer, O. S., Diller, L. C., Brainard D. H., Peterson, B. B., Lee, B. B. (2000b).
Center-surround receptive field structure of cone bipolar cells in primate retina.
Vision Research **40**(14): 1801-1811.
- Dartnall, H. J., Bowmaker, J. K., Mollon, J. D. (1983)
Human visual pigments: microspectrophotometric results from the eyes of seven persons.
Proceedings of the Royal Society of London. Series B, Biological Sciences **220**(1218): 115-130.
- Dawson, W. W., Trick, G. L., Litzkow, C. A. (1979)
Improved electrode for electroretinography.
Investigative Ophthalmology and Visual Science **18**: 988-991.
- Dawson, W. W., Trick, G. L., Maida, T. M. (1982)
Evaluation of the DTL-corneal electrode.
Documenta Ophthalmologica **31**: 81-88.
- Deeb, S. S., Diller, L. C., Williams, D. R., Dacey, D. M. (2000)
Interindividual and topographical variation of L:M cone ratios in monkey retinas.
Journal of the Optical Society of America. A, Optics, Image Science, and Vision **17**(3): 538-544.
- Derrington, A. M., Krauskopf, J., Lennie, P. (1984)
Chromatic mechanisms in lateral geniculate nucleus of macaque.
Journal of Physiology **357**: 241-265.
- Derrington, A. M., Lennie, P. (1984)
Spatial and temporal contrast sensitivities of neurons in lateral geniculate nucleus of macaque.
Journal of Physiology **357**: 219-240.
- De Valois, R. L., De Valois, K. K. (1993)
A multi-stage color model.
Vision Research **33**(8): 1053-1065.

- De Vries (1946)
Luminosity curves of trichromats.
Nature **157**: 736-737.
- Dobkins, K. R., Thiele, A., Albright, T. D. (2000)
Comparison of red-green equiluminance points in humans and macaques: evidence for different L:M cone ratios between species.
Journal of the Optical Society of America. A, Optics, Image Science, and Vision **17**(3): 545-556.
- Estevez, O., Spekreijse, H. (1982)
The "silent substitution" method in visual research.
Vision Research **22**(6): 681-691.
- Famiglietti, E. V., Jr., Kolb, H. (1976)
Structural basis for ON-and OFF-center responses in retinal ganglion cells.
Science **194**(4261): 193-195.
- Gouras, P. (1971)
The function of the midget cell system in primate color vision.
Vision Research Supplement **3**: 397-410.
- Gouras, P. (1984)
Color Vision.
Progress in Retinal Research **3**: 227-261.
- Guth, S. L., Alexander, J. V., Chumbly, J. I., Gillman, C. B., Patterson, M. M. (1968)
Factors affecting luminance additivity at threshold among normal and color-blind subjects and elaborations of a trichromatic-opponent colors theory.
Vision Research **8**(7): 913-928.
- Hagstrom, S. A., Neitz, J., Neitz, M. (1998)
Variations in cone populations for red-green color vision examined by analysis of mRNA.
Neuroreport **9**(9): 1963-1967.
- Hagstrom, S. A., Neitz, M., Neitz, J. (2000)
Cone pigment gene expression in individual photoreceptors and the chromatic topography of the retina.
Journal of the Optical Society of America. A, Optics, Image Science, and Vision **17**(3): 527-537.
- Halliday, A. M., McDonald, W. I., Mushin, J. (1973)
Visual evoked response in diagnosis of multiple sclerosis.
British Medical Journal **4**(5893): 661-664.

- Harding, G. F., Odom, J. V., Spileers, W., Spekreijse, H. (1996)
Standard for visual evoked potentials 1995. The International Society for
Clinical Electrophysiology of Vision.
Vision Research **36**(21): 3567-3572.
- Hare, W. A., Ton, H., Ruiz, G., Feldmann, B., Wijono, M., WoldeMussie, E.
(2001)
Characterization of retinal injury using ERG measures obtained with both
conventional and multifocal methods in chronic ocular hypertensive
primates.
Investigative Ophthalmology and Visual Science **42**(1): 127-136.
- Hood, D. C., Seiple, W., Holopigian, K., Greenstein, V. (1997)
A comparison of the components of the multifocal and full-field ERGs.
Visual Neuroscience **14**(3): 533-544.
- Hood, D. C. (2000)
Assessing retinal function with the multifocal technique.
Progress in Retinal Research **19**(5): 607-646.
- Hood, D. C., Odel, J. G., Zhang, X. (2000a)
Tracking the recovery of local optic nerve function after optic neuritis: a
multifocal VEP study.
Investigative Ophthalmology and Visual Science **41**(12): 4032-4038.
- Hood, D. C., Zhang, X. (2000)
Multifocal ERG and VEP responses and visual fields: comparing disease-
related changes.
Documenta Ophthalmologica **100**(2-3): 115-137.
- Hood, D. C., Zhang, X., Greenstein, V. C., Kangovi, S., Odel, J. G., Liebmann,
J. M., Ritch, R. (2000b)
An interocular comparison of the multifocal VEP: a possible technique for
detecting local damage to the optic nerve.
Investigative Ophthalmology and Visual Science **41**(6): 1580-1587.
- Hood, D. C., Frishman, L. J., Saszik, S., Viswanathan, S. (2002a)
Retinal origins of the primate multifocal ERG: implications for the human
response.
Investigative Ophthalmology and Visual Science **43**(5): 1673-1685.
- Hood, D. C., Zhang, X., Hong, J. E., Chen, C.S. (2002b)
Quantifying the benefits of additional channels of multifocal VEP
recording.
Documenta Ophthalmologica **104**(3): 303-320.

- Hood, D. C., Yu, A. L., Zhang, X., Albrecht, J., Jägle, H., Sharpe, L. T. (2002c)
The multifocal visual evoked potential and cone-isolating stimuli:
Implications for L- to M-cone ratios and normalization.
Journal of Vision **2**(2): 178-189.
- Horiguchi, M., Suzuki, S., Kondo, M., Tanikawa, A., Miyake, Y. (1998)
Effect of glutamate analogues and inhibitory neurotransmitters on the
electroretinograms elicited by random sequence stimuli in rabbits.
Investigative Ophthalmology and Visual Science **39**(11): 2171-2176.
- Jacobs, G. H., Neitz, J., Krogh, K. (1996)
Electroretinogram flicker photometry and its applications.
*Journal of the Optical Society of America. A, Optics, Image Science, and
Vision* **13**(3): 641-648.
- Jacoby, R., Stafford, D., Kouyama, N., Marshak, D. (1996)
Synaptic inputs to ON parasol ganglion cells in the primate retina.
Journal of Neuroscience **16**: 8041-8056.
- Kaneko, A. (1970)
Physiological and morphological identification of horizontal, bipolar and
amacrine cells in goldfish retina.
Journal of Physiology, London **207**: 623-633.
- Klistorner, A. I., Graham, S. L., Grigg, J. R., Billson, F. A. (1998)
Multifocal topographic visual evoked potential: improving objective
detection of local visual field defects.
Investigative Ophthalmology and Visual Science **39**(6): 937-950.
- Klistorner, A. I., Graham, S. L. (1999)
Multifocal pattern VEP perimetry: analysis of sectoral waveforms.
Documenta Ophthalmologica **98**(2): 183-196.
- Klistorner, A., Graham, S. L. (2000)
Objective perimetry in glaucoma.
Ophthalmology **107**(12): 2283-2299.
- Kolb, H. (1970)
Organization of the outer plexiform layer of the primate retina: electron
microscopy of Golgi-impregnated cells.
Philosophical Transactions of the Royal Society of London. Series B **258**:
261-283.
- Kolb, H., Dekorver, L. (1991)
Midget ganglion cells of the parafovea of the human retina: a study by
electron microscopy and serial section reconstructions.
Journal of Comparative Neurology **303**(4): 617-636.

- Kouyama, N., Marshak, D. W. (1992)
Bipolar cells specific for blue cones in the macaque retina.
Journal of Neuroscience **12**: 1233-1252.
- Krauskopf, J., Williams, D. R., Heeley, D. W. (1982)
Cardinal directions of color space.
Vision Research **22**:1123-1131.
- Krauskopf, J. (2000)
Relative number of long- and middle-wavelength-sensitive cones in the human fovea.
Journal of the Optical Society of America. A, Optics, Image Science, and Vision **17**(3): 510-516.
- Kremers, J., Usui, T., Scholl, H. P., Sharpe, L. T. (1999)
Cone signal contributions to electroretinograms [correction of electrograms] in dichromats and trichromats.
Investigative Ophthalmology and Visual Science **40**(5): 920-930.
- Kremers, J., Scholl, H. P., Knau, H., Berendschot, T. T., Usui, T., Sharpe, L.T. (2000)
L/M cone ratios in human trichromats assessed by psychophysics, electroretinography, and retinal densitometry.
Journal of the Optical Society of America. A, Optics, Image Science, and Vision **17**(3): 517-526.
- Kuffler, S. W. (1953)
Discharge patterns and functional organization of mammalian retina.
Journal of Neurophysiology **16**: 37-68.
- Lee, B. B., Pokorny, J., Smith, V. C., Martin, P. R., Valberg, A. (1990)
Luminance and chromatic modulation sensitivity of macaque ganglion cells and human observers.
Journal of the Optical Society of America. A, Optics, Image Science, and Vision **7**(12): 2223-2236.
- Lennie, P., Haake, P. W., Williams, D. R. (1991)
The design of chromatically opponent receptive fields.
In: Landy, M. S., Movshon, J. A. (eds.): *Computational Models of Visual Processing*, pp. 71-82.
MIT Press, Cambridge, MA.
- Lynch, J. J., Silveira, L. C. L., Perry, V. H., Merigan, W. H. (1992)
Visual effects of damage to P ganglion cells in macaques.
Visual Neuroscience **8**: 575-583.

- Martin, P. R., White, A. J. R., Goodchild, A. K., Wilder, H. D., Sefton, A. E. (1997)
Evidence that blue-ON cells are part of the third geniculocortical pathway in primates.
European Journal of Neuroscience **9**: 1536-1541.
- Merigan, W. (1989)
Chromatic and achromatic vision of macaques: role of the P pathway.
Journal of Neuroscience **9**: 776-783.
- Milam A. H., Dacey, D. M., Dizhoor, A. M. (1993)
Recoverin immunoreactivity in mammalian cone bipolar cells.
Visual Neuroscience **10**: 1-12.
- Mitchell, D. E., Rushton, W. A. H. (1971a)
Visual pigments in dichromats.
Vision Research **11**: 1033-1043.
- Mitchell, D. E., Rushton, W. A. H. (1971b)
The red/green pigments of normal vision.
Vision Research **11**: 1045-1056.
- Mullen, K. T., Kingdom, F. A. (1996)
Losses in peripheral colour sensitivity predicted from "hit and miss" post-receptoral cone connections.
Vision Research **36**(13): 1995-2000.
- Nathans, J., Piantanida, T. P., Eddy, R. L., Shows, T. B. (1986a)
Molecular genetics of inherited variation in human color vision.
Science **232**: 203-210.
- Nathans, J., Thomas, D., Hogness, D. S. (1986b)
Molecular genetics of human color vision: the genes encoding blue, green, and red pigments.
Science **232**: 193-202.
- Nelson, R., Famiglietti, E. V., Jr., Kolb, H. (1978)
Intracellular staining reveals different levels of stratification for on- and off-center ganglion cells in cat retina.
Journal of Neurophysiology **41**(2): 472-483.
- Nelson, R., Kolb, H. (1983)
Synaptic patterns and response properties of bipolar and ganglion cells in the cat retina.
Vision Research **23**: 1183-1195.

- Osterberg, G. (1935)
 Topography of the layer of rods and cones in the human retina.
Acta Ophthalmologica (suppl.) **6**: 1-103.
- Otake, S., Cicerone, C. M. (2000)
 L and M cone relative numerosity and red-green opponency from fovea to midperiphery in the human retina.
Journal of the Optical Society of America. A, Optics, Image Science, and Vision **17**(3): 615-627.
- Perry, V. H., Oehler, R., Cowey, A. (1984)
 Retinal ganglion cells that project to the dorsal lateral geniculate nucleus in the macaque monkey.
Neuroscience **12**: 1101-1123.
- Pokorny, J., Smith, V. C., Wesner, M. F. (1991)
 Variability in cone populations and implications.
 In: Valberg, A., Lee B. B. (eds.): *From pigments to perception: Advances in understanding visual processes*, pp.1-9.
 Plenum Press, New York.
- Polyak, S. L. (1941)
 In: *The Retina*.
 University of Chicago Press, Chicago.
- Pugh E. N. (1988)
 Physics and retinal physiology.
 In: Atkinson R. C. (ed.): *Stevens Handbook of Experimental Psychology*.
 Wiley, New York.
- Purpura, K., Kaplan, E., Shapley, R. M. (1988)
 Background light and the contrast gain of primate P and M retinal ganglion cells.
Proceedings of the National Academy of Sciences of the United States of America **85**: 4534-4537.
- Roorda, A., Williams, D. R. (1999)
 The arrangement of the three cone classes in the living human eye.
Nature **397**(6719): 520-522.
- Rushton, W. A., Baker, H. D. (1964)
 Red-green sensitivity in normal vision.
Vision Research **4**(1): 75-85.
- Scar, G., Maunsell, J. H. R., Lennie, P. (1990)
 Coding of image contrast in central visual pathways of the macaque monkey.
Vision Research **30**: 1-10.

- Schiller, P. H., Colby, C.L. (1983)
The responses of single cells in the lateral geniculate nucleus of the rhesus monkey to color and luminance contrast.
Vision Research **23**: 1631-1641.
- Schiller, P. H., Logothetis, N. K., Charles, E. R. (1991)
Parallel pathways in the visual system: their role in perception at isoluminance.
Neuropsychologia **29**: 433-441.
- Sieving, P. A., Murayama, K., Naarendorp, F. (1994)
Push-pull model of the primate photopic electroretinogram: a role for hyperpolarizing neurons in shaping the b-wave.
Visual Neuroscience **11**(3): 519-532.
- Slotnick, S. D., Klein, S. A., Carney, T., Sutter, E., Dastmalchi, S. (1999)
Using multi-stimulus VEP source localization to obtain a retinotopic map of human primary visual cortex.
Clinical Neurophysiology **110**(10): 1793-1800.
- Smith, V. C., Pokorny, J. (1975)
Spectral sensitivity of the foveal cone photopigments between 400 and 500 nm.
Vision Research **15**(2): 161-171.
- Solomon, S. G., White A. J., Martin P. R. (1999)
Temporal contrast sensitivity in the lateral geniculate nucleus of a New World monkey, the marmoset *Callithrix jacchus*.
Journal of Physiology **517**(3): 907-917.
- Stiles, W.S. (1978)
Further studies of visual mechanisms by the two-colour threshold method.
In: *Colloquio sobre Problemas Opticos de la Vision* (n.p., Madrid, 1953), Vol. 1, pp.65-103; reprinted in W. S. Stiles, *Mechanisms of Colour Vision* (Academic, New York, 1978).
- Stockman, A., MacLeod, D. I. A., DePriest, D. D. (1991)
The temporal properties of the human short-wave photoreceptors and their associated pathways.
Vision Research **31**: 189-208.
- Stockman, A., MacLeod, D. I., Johnson, N. E. (1993)
Spectral sensitivities of the human cones.
Journal of the Optical Society of America. A, Optics, Image Science, and Vision **10**(12): 2491-2521.

- Stockman, A., Sharpe, L. T. (1998)
Human cone spectral sensitivities: a progress report.
Vision Research **38**(21): 3193-3206.
- Stockman, A., Sharpe, L. T. (1999)
Cone spectral sensitivities and color matching.
In: Gegenfurtner, K., Sharpe, L. T. (eds.): Color Vision: From Genes to Perception, pp. 53-88.
Cambridge U. Press, Cambridge, UK.
- Stockman, A., Sharpe, L. T. (2000)
The spectral sensitivities of the middle- and long-wavelength-sensitive cones derived from measurements in observers of known genotype.
Vision Research **40**(13): 1711-1737.
- Sutter, E. E., Tran, D. (1992)
The field topography of ERG components in man--I. The photopic luminance response.
Vision Research **32**(3): 433-446.
- Sutter, E. E., Bearnse, M. A., Jr. (1999)
The optic nerve head component of the human ERG.
Vision Research **39**(3): 419-436.
- Sutter, E. E., Shimada, Y., Li, Y., Bears, M. A. (1999)
Mapping inner retinal function through enhancement of adaptive component in the mERG.
In: Vision Science and its Applications, OSA Tech Dig Ser 1 (Optical Society of America, Washington DC), pp: 52-55.
- Sutter, E. E. (2000)
The interpretation of multifocal binary kernels.
Documenta Ophthalmologica **100** (2/3): 49-75.
- Teping, C. (1981)
Visusbestimmung mit Hilfe des visuell evozierten kortikalen Potentials (VECP).
Klinische Monatsblätter fuer Augenheilkunde: 179-169.
- Tsukamoto, Y., Masarachia, P., Schein, S. J., Sterling, P. (1992)
Gap junctions between the pedicles of macaque foveal cones.
Vision Research **32**: 1809-1815.
- van de Kraats, J., Berendschot, T. T., van Norren, D. (1996)
The pathways of light measured in funds reflectometry.
Vision Research **36**(15): 2229-2247.

- von Helmholtz, H. (1852)
On the theory of compound colours.
Philosophical Magazine, Serial 4, **4**: 519-535.
- Vos, J. J., Walraven, P. L. (1971)
On the derivation of the foveal receptor primaries.
Vision Research **11**(8): 799-818.
- Wesner, M. F., Pokorny, J., Shevell, S. K., Smith, V. C. (1991)
Foveal cone detection statistics in color-normals and dichromats.
Vision Research **31**(6): 1021-1037.
- White, A. J. R., Wilder, H. D., Goodchild, A. K., Sefton, A. J., Martin, P. R. (1998)
Segregation of receptive field properties in the lateral geniculate nucleus of a new-world monkey, the marmoset *Callithrix jacchus*.
Journal of Neurophysiology **80**: 2063-2076.
- Wikler, K. C., Rakic, P. (1990)
Distribution of photoreceptor subtypes in the retina of diurnal and nocturnal primates.
Journal of Neuroscience **10**: 3390-3401.
- Wyszecki, G., Stiles, W. S. (1982)
Color science: Concepts and methods, quantitative data and formulae.
Wiley, New York, Chichester, Brisbane, Toronto, Singapore.
- Young, T. (1802)
On the theory of light and colors.
Philosophical Transactions of the Royal Society **91**:12-49.

Acknowledgments

I would like to acknowledge my great indebtedness to Professor Dr. E. Zrenner for leaving the topic of this doctoral thesis with me and enabling me to spend a sojourn at Columbia University, New York, NY, U.S.A..

I owe an equally great debt to Professor Dr. D. C. Hood, with whom I conducted the majority of the experiments, and who was invaluable in providing support at all stages of this work. I especially would like to thank him for his intensive personal assistance and for being such an excellent mentor.

I am immensely grateful to Professor Dr. Lindsay T. Sharpe for his scientific and strategic advices during this work and for his help and encouragement to apply for this sojourn.

I give gratitude to Dr. H. Jäggle for his patience to look through my manuscripts and making the proper corrections, without which this thesis could not be completed.

Special thanks goes to J. Albrecht and X. Zhang for introducing me into the silent substitution method and into their programming work and for providing me with their many advices and technical support.

I am also indebted to all the participants of this study for their time and efforts, which only made this study possible.

Thank you very much also to the Deutsche Akademische Auslandsdienst (DAAD), which provided me with a stipend for this sojourn.

And lastly, I would like to thank my parents for their perpetual encouragement and their financial support.

Curriculum Vitae

Name: Yu, Alice Lap-Ho
Date and Place of Birth: 07th October 1976 in Hongkong
Marital Status: single
Parents: Ping-Pok Yu, M.D.; Kin-Fan Ku, M.D.

School:

1983 – 1987 Kasteneckschule in Freiberg a.N. (elementary school)
1987 – 1996 Oscar-Paret-Schule in Freiberg a.N. (,Gymnasium'),
graduating with ,Abitur'

Medical Studies:

04/97 Start of medical studies at the Eberhard-Karls-Universität
Tübingen
03/99 Ärztliche Vorprüfung (preclinical exam)
03/00 1. Abschnitt der Ärztlichen Prüfung (1st clinical exam)
09/00 – 04/01 Research scholar at Columbia University, New York, NY,
U.S.A.
04/01 Continued medical studies at the Ludwig-Maximilians-
Universität München
03/02 2. Abschnitt der Ärztlichen Prüfung (2nd clinical exam)
04/02 – 08/02 1. PJ-Tertial (1st clinical clerkship) at Harvard Medical
School, Boston, MA, U.S.A.
08/02 – 11/02 2. PJ-Tertial (2nd clinical clerkship) at Universitäts-
Augenklinik – Innenstadt, München
12/02 – 03/03 3. PJ-Tertial (3rd clinical clerkship) at Chirurgische Klinik
und Poliklinik, Großhadern, München
04th June 2003 3. Abschnitt der Ärztlichen Prüfung (3rd clinical exam)

